

Dear Dr. Kerminen,

Thank you for obtaining the review comments of our revised manuscript. We have addressed all the comments and revised the manuscript accordingly, as detailed below. All changes made to the manuscript have been marked with Track-Change tool in one of submitted files.

Please let me know if there are any questions.

Best regards,

Fangqun Yu

Comments on the revised manuscript by Yu et al.

The authors thank the referee again for taking time to review the revised manuscript and provide constructive comments, which have allowed us to further clarify and improve the manuscript. Our point-to-point replies to the comments are given below, with the original comments in black, and our response in blue.

I'm happy to see that the authors have included more data in the measurement comparisons, and also made the discussion more balanced. I have one main suggestion regarding the new comparison (Figure 8):

As discussed, the agreement between CLOUD measurements and the presented model becomes worse when (1) temperature increases, and (2) ions are not present. It would be good to note that these are the conditions when the role of cluster evaporation (i.e. thermodynamics) becomes more important (i.e. higher evaporation and/or generally less tightly bound clusters), and thus they are likely to reveal the biases of the used thermochemistry. This naturally applies to all thermodynamic data sets, PW91PW91/6-311++G(3df,3pd) and other, regardless of the kinetic model framework used.

Agree. We have pointed this out in the revised manuscript.

Also, will the model be freely available?

The model is presently not yet in the public domain. We will continue to evaluate and improve the model by comparing with more measurements (including those taken in the atmosphere). On the other hand, we will make the parameterization of TIMN based on the present model available to the community (in term of lookup tables) after the publication of this manuscript. The TIMN parameterization can be easily used in 3-D models to calculate TIMN rates under a wide range of atmospheric conditions.

In addition, some of the replies to my previous comments were slightly inadequate. For instance, the following points would still need a bit of elaboration:

Comment on the model being quasi-unary: The authors reply that “the model is multicomponent” - I agree that the thermodynamic data is multi-component, but the kinetic model is not. The kinetic equations consider only the number of H<sub>2</sub>SO<sub>4</sub> molecules  $i$  in each particle (page 7): “ $N_i$  is the total number concentration (cm<sup>-3</sup>) of all cluster/particles (binary +

ternary) in the bin  $i$ . For small clusters ( $i \leq 10$ ),  $N_i$  is the number concentration ( $\text{cm}^{-3}$ ) of all clusters containing  $i$   $\text{H}_2\text{SO}_4$  molecules.” To the best of my knowledge, this means that the model is quasi-unary, and also the authors have used the same term for the previous versions of the model (Yu, J. Chem. Phys., 127, 054301, 2007). If the model was explicitly multi-component, then there would be no reason to apply the equilibrium assumptions for e.g. ammonia.

We respect this different perspective with regard to quasi-unary. It does not affect the findings and conclusions of the present work.

Comment 1: I did not ask about the QC data, I asked if the different approaches to assess the thermochemistry of clusters and particles of different sizes, compositions and charging states (QC, Eq. (10), experimental liquid data...) could be presented in an easy-to-read way. How about including this information e.g. in Figure 1? That is, explain for each charging state which size range is described with which thermochemical data; it would be much easier than digging the information from the text.

Our fault for the mis-interpretation of the comment. Actually this information can be readily found in Fig. 4a where the clusters using QC data are marked with symbols and those based on Eq (10) and experimental liquid data are described in Figure caption. To mark “QC, Eq. (10), experimental liquid data” in Figure 1 will make Figure 1 too busy. Therefore we didn’t modify Figure 1.

Comment 17: I don’t understand why you artificially set the cumulative Gibbs free energy to zero when it should be negative. Free energy profiles exhibiting both a minimum and a maximum can naturally occur, especially for charged clusters (see e.g. Figure 2 in Vehkamäki and Riipinen, Chem. Soc. Rev. 41, 5160-5173, 2012), and it simply means that there exist stable “pre-nucleation” clusters.

Got the point. To address the referee’s concern, we have updated Fig. 4 for negative ions to include the negative  $\Delta G$  in accumulative Gibbs free energy. The change is just for the approach to present and does not affect the TIMN rates. The related text is also updated accordingly.

Comment 18: The vapor concentrations were probably also used to convert the QC data to the given conditions (through the law of mass action)?

Yes.

Comment 24: I understand that parameter  $c$  is an approximation, but the statement “We estimated  $c$  based on QC data” still does not answer the question about how  $c$  is exactly calculated.

As stated in the text (Lines 388-391), “In the present study,  $c$  is estimated from  $\Delta G_{s-1,s}$  at  $s=2$  and  $s=3$  for neutral binary and ternary clusters for which experimental (Hanson and Lovejoy, 2006; Kazil et al., 2007) or quantum-chemical data (Table A3) are available”. We feel that this explains how  $c$  is calculated. We slightly modified the sentence to make it clearer.

“In the present study,  $c$  is estimated by fitting  $\Delta G_{s-1,s}$  at  $s=2$  and  $s=3$  based on Eq. (10) to those from experimental (Hanson and Lovejoy, 2006; Kazil et al., 2007) or quantum-chemical data (Table A3).”

Comment 25: I fully agree that “the formation of small clusters are limiting steps”, but the particle formation process is limited by cluster stability throughout the size range where the clusters are not stable, which is at least up to the barrier maximum. This is clear e.g. from simplified kinetic models such as classical nucleation theory, where the cluster free energy at the maximum of the barrier (the “critical cluster”) is the only free energy determining the particle formation rate. I am sure the authors agree, since they have recently used such critical-cluster-based approaches themselves (Yu et al., Atmos. Chem. Phys. 17, 4997-5005, 2017).

Also, repeating that the model is “in excellent agreement with CLOUD measurements” is not helpful, when Figure 8 tells that this is not the case in all conditions. Thus, there is no need to commend a model when it is not justifiable, but it is instead good to point out the weaker features (as the authors already have nicely done in replies to some other comments).

We agree with the referee that “the particle formation process is limited by cluster stability throughout the size range where the clusters are not stable”. When we say that “the formation of small clusters are limiting steps”, we mean that the cluster free energy at the maximum of the barrier (the “critical cluster”) is dominated by small clusters.

We searched the whole manuscript, only in one place (line 22) we found “in excellent agreement with CLOUD measurements”. However, this statement refers to “The model reveals the general favor of nucleation of negative ions, followed by nucleation on positive ions and neutral nucleation, for which higher NH<sub>3</sub> concentrations are needed,” (Lines 20-22). Therefore, this statement is justified.

We agree that Figure 8 shows the difference between model prediction and CLOUD measurements for neutral nucleation at high temperature. This has been pointed out in the text, along with possible reasons. It should be noted that in the real atmosphere ionization is always present and under such a condition TIMN model is overall in excellent agreement with CLOUD measurements.

Comment 26: It might be good to clearly note then, that the model scheme is probably not suitable for situations where ammonia concentration is not substantially higher than H<sub>2</sub>SO<sub>4</sub> concentration.

To address the referee’s concern, the sentence (Line 304) has been modified to clearly note this.

To amend a few issues:

“Please note that the nucleation rates measured in CLOUD are also steady state values”:

Equilibrium and steady state are two different things, and the fact that CLOUD formation rates are assessed for a steady state has nothing to do with the assumption regarding cluster equilibration with respect to ammonia. (Equilibrium is a steady state with no net formation or growth of particles. A steady state where particle formation occurs is not equilibrium, but instead any time-independent situation with or without cluster equilibration with respect to some chemical compound.)

Got the point.

“It should be noted that all previous ternary nucleation models discussed in Section 2.1 assume the equilibrium with respect to NH<sub>3</sub>”: No, they actually don’t. For instance, the acid-base

scheme used by Chen et al. (Proc. Nat. Acad. Sci., 109, 18713-18718, 2012), and further developed by Jen et al. (J. Geophys. Res. Atmos., 119, 7502-7514, 2014), assumes two separate acid dimers (clusters containing two acid molecules) that have different base content. ACDC (McGrath et al., Atmos. Chem. Phys., 12, 2345-2355, 2012) does not make any equilibrium assumptions with respect to ammonia.

We meant all previous CLASSICAL ternary nucleation models discussed in Section 2.1., Coffman and Hegg, 1995; Korhonen et al., 1999; Napari et al., 2002.

Got the referee's point with regard to the equilibrium assumption. No change is needed for the text as the above comments refer to the discussion in our previous reply to the referee's comments.

Comment 27: Please add these clarifications also to the manuscript (I was not able to find them there).

Yes. These clarifications are now included in the revised manuscript.

Comment 28: If Eqs. (1) and (2) correspond to  $H^+AaWw$  and  $NO_3^-$ , in which equation is the bisulfate ion  $HSO_4^-$  included, i.e. does index  $i$  in Eq. (5) refer to the sum of  $H_2SO_4$  and  $HSO_4^-$ ? What does the second term of Eq. (2) describe; is  $NO_3^-$  evaporating from a negative cluster or  $HSO_4^-$ ?

Yes, index  $i$  in Eq. (5) refers to the sum of  $H_2SO_4$  and  $HSO_4^-$ . The second term of Eq. (2) describes the reaction of  $HSO_4^- + HNO_3 \rightarrow NO_3^- + H_2SO_4$ . Although the rate of this reaction is generally negligible, we keep the term there for completeness. We have clarified these in the text (Lines 194-196).

Comment 29: Yes, but isn't the double count canceled also for the evaporation term? This is because the evaporation rate constant  $\gamma$  \*includes\* the collision rate constant  $\beta$  as given by Eq. (7), and the permutation factor of 1/2 should be included in  $\beta$ . Or is the  $\beta$  in Eq. (7) defined differently than the  $\beta$  in Eq. (3)?

The  $\beta$  in Eq. (7) is the same as the  $\beta$  in Eq. (3). In our definition,  $\beta$ , as defined in reference cited (Yu, 2007), is simply the collision rate constant and does not contain the permutation factor of 1/2. Therefore, Eq. (3) is correct.

Comment 31: There's something wrong with the updated Eqs. (7) and (8), since the  $H_2SO_4$  concentration  $N_{1,0}$  doesn't cancel out; please fix this. In any case, there is no reason to include any  $H_2SO_4$  concentrations in the equation of evaporation rate, as they are not needed there. The original comment was mainly related to the statement "N0 is the number concentration of  $H_2SO_4$  at a given T under the reference vapor pressure P of 1 atm". In QC methods, N0 is the arbitrary number concentration of a hypothetical gas consisting solely of the species for which the calculation is performed (which can be a single molecule or a cluster), and doesn't have to do with any concrete  $H_2SO_4$  or other vapor concentration. Conversions are not needed, as they cancel out in the evaporation rate anyway, as the authors state.

The referee is correct. We have changed Eq. (8) back to the original one (as in ACPD) and pointed out that N0 is the arbitrary number concentration of a hypothetical gas consisting solely

of the species for which the calculation is performed (generally under the reference vapor pressure  $P$  of 1 atm).

Comment 43: It is still claimed in Section 3 of the revised manuscript (page 18, line 554) that the ACDC model neglects the effect of water.

We have deleted the phrase “(which is neglected in both the CLOUDpara and ACDC models)” from the sentence.

1 **H<sub>2</sub>SO<sub>4</sub>-H<sub>2</sub>O-NH<sub>3</sub> ternary ion-mediated nucleation (TIMN): Kinetic-based model and**  
2 **comparison with CLOUD measurements**

3  
4 Fangqun Yu<sup>1</sup>, Alexey B. Nadykto<sup>1,2</sup>, Jason Herb<sup>1</sup>, Gan Luo<sup>1</sup>, Kirill M. Nazarenko<sup>2</sup>, and  
5 Lyudmila A. Uvarova<sup>2</sup>

6 Correspondence to: F. Yu ([fyu@albany.edu](mailto:fyu@albany.edu))

7  
8 <sup>1</sup> Atmospheric Sciences Research Center, University at Albany, Albany, New York, US

9 <sup>2</sup> Department of Applied Mathematics, Moscow State Univ. of Technology “Stankin”, Russia

10  
11  
12 **Abstract.** New particle formation (NPF) is known to be an important source of atmospheric  
13 particles that impacts air quality, hydrological cycle, and climate. Although laboratory  
14 measurements indicate that ammonia enhances NPF, the physico-chemical processes underlying  
15 the observed effect of ammonia on NPF are yet to be understood. Here we present a comprehensive  
16 kinetically-based H<sub>2</sub>SO<sub>4</sub>-H<sub>2</sub>O-NH<sub>3</sub> ternary ion-mediated nucleation (TIMN) model that is based  
17 on the thermodynamic data derived from both quantum-chemical calculations and laboratory  
18 measurements. NH<sub>3</sub> was found to reduce nucleation barriers for neutral, positively charged, and  
19 negatively charged clusters differently, due to large differences in the binding strength of NH<sub>3</sub>,  
20 H<sub>2</sub>O, and H<sub>2</sub>SO<sub>4</sub> to small clusters of different charging states. The model reveals the general favor  
21 of nucleation of negative ions, followed by nucleation on positive ions and neutral nucleation, for  
22 which higher NH<sub>3</sub> concentrations are needed, in excellent agreement with Cosmics Leaving  
23 Outdoor Droplets (CLOUD) measurements. The TIMN model explicitly resolves dependences of  
24 nucleation rates on all the key controlling parameters, and captures well the absolute values of  
25 nucleation rates as well as the dependence of TIMN rates on concentrations of NH<sub>3</sub> and H<sub>2</sub>SO<sub>4</sub>,  
26 ionization rates, temperature, and relative humidity observed in the well-controlled CLOUD  
27 measurements. The kinetic model offers physico-chemical insights into the ternary nucleation  
28 process and provides a physics-based approach to calculate TIMN rates under a wide range of  
29 atmospheric conditions.

30

## 31 **1. Introduction**

32 New particle formation (NPF), an important source of particles in the atmosphere, is a dynamic  
33 process involving interactions among precursor gas molecules, small clusters, and pre-existing  
34 particles (Yu and Turco, 2001; Zhang et al., 2012).  $\text{H}_2\text{SO}_4$  and  $\text{H}_2\text{O}$  are known to play an important  
35 role in atmospheric particle formation (e.g., Doyle, 1961). In typical atmospheric conditions, the  
36 species dominating the formation and growth of small clusters is  $\text{H}_2\text{SO}_4$ . The contribution of  $\text{H}_2\text{O}$   
37 to the nucleation is related to the hydration of  $\text{H}_2\text{SO}_4$  clusters (or, in the other words, modification  
38 of the composition of nucleating clusters) that reduces the  $\text{H}_2\text{SO}_4$  vapor pressure and hence  
39 diminishes the evaporation of  $\text{H}_2\text{SO}_4$  from the pre-nucleation clusters.  $\text{NH}_3$ , the most abundant  
40 gas-phase base molecule in the atmosphere and a very efficient neutralizer of sulfuric acid  
41 solutions, has long been proposed to enhance nucleation in the lower troposphere (Coffman and  
42 Hegg, 1995) although it has been well recognized that earlier versions of classical ternary  
43 nucleation model (Coffman and Hegg, 1995; Korhonen et al., 1999; Napari et al., 2002)  
44 significantly over-predict the effect of ammonia (Yu, 2006a; Merikanto et al., 2007; Zhang et al.,  
45 2010).

46 The impacts of  $\text{NH}_3$  on NPF have been investigated in a number of laboratory studies (Kim et  
47 al., 1998; Ball et al., 1999; Hanson and Eisele, 2002; Benson et al., 2009; Kirkby et al., 2011;  
48 Zollner et al., 2012; Froyd and Lovejoy, 2012; Glasoe et al., 2015; Schobesberger et al., 2015;  
49 Kurten et al., 2016) including those recently conducted at the European Organization for Nuclear  
50 Research (CERN) in the framework of the CLOUD (Cosmics Leaving Outdoor Droplets)  
51 experiment that has provided a unique dataset for quantitatively examining the dependences of  
52 ternary  $\text{H}_2\text{SO}_4$ - $\text{H}_2\text{O}$ - $\text{NH}_3$  nucleation rates on concentrations of  $\text{NH}_3$  ( $[\text{NH}_3]$ ) and  $\text{H}_2\text{SO}_4$   
53 ( $[\text{H}_2\text{SO}_4]$ ), ionization rate (Q), temperature (T), and relative humidity (RH) (Kirkby et al., 2011;  
54 Kurten et al., 2016). The experimental conditions in the CLOUD chamber, a 26.1 m<sup>3</sup> stainless steel  
55 cylinder, were well controlled, while impacts of potential contaminants were minimized  
56 (Schnitzhofer et al., 2014; Duplissy et al., 2016). Based on CLOUD measurements in  $\text{H}_2\text{SO}_4$ - $\text{H}_2\text{O}$ -  
57  $\text{NH}_3$  vapor mixtures, Kirkby et al. (2011) reported that an increase of  $[\text{NH}_3]$  from  $\sim 0.03$  ppb (parts  
58 per billion, by volume) to  $\sim 0.2$  ppb can enhance ion-mediated (or induced) nucleation rate by 2-3  
59 orders of magnitude and that the ion-mediated nucleation rate is a factor of 2 to  $>10$  higher than  
60 that of neutral nucleation under typical level of contamination by amines. In the presence of  
61 ionization, highly polar common atmospheric nucleation precursors such as  $\text{H}_2\text{SO}_4$ ,  $\text{H}_2\text{O}$ , and  $\text{NH}_3$   
62 molecules tend to cluster around ions; and charged clusters are generally much more stable than  
63 their neutral counterparts with enhanced growth rates as a result of dipole-charge interactions (Yu  
64 and Turco, 2001).

65 Despite of various laboratory measurements indicating that ammonia enhances NPF, the  
66 physico-chemical processes underlying the observed different effects of ammonia on the formation  
67 of neutral, positively charged and negatively charged clusters (Schobesberger et al., 2015) are yet  
68 to be understood. To achieve such an understanding, a nucleation model based on the first  
69 principles is needed. Such a model is also necessary to extrapolate data obtained in a limited  
70 number of experimental conditions to a wide range of atmospheric conditions, where  $[\text{NH}_3]$ ,  
71  $[\text{H}_2\text{SO}_4]$ , ionization rates, T, RH and surface areas of preexisting particles vary widely depending  
72 on the region, pollution level and season. The present work aims to address these issues by  
73 developing a kinetically-based  $\text{H}_2\text{SO}_4\text{-H}_2\text{O-NH}_3$  ternary ion-mediated nucleation (TIMN) model  
74 that is based on the molecular clustering thermodynamic data. The model predictions are compared  
75 with relevant CLOUD measurements and previous studies.

76

## 77 **2. Kinetic-based $\text{H}_2\text{SO}_4\text{-H}_2\text{O-NH}_3$ ternary ion-mediated nucleation (TIMN) model**

### 78 2.1. Background

79 Most nucleation models developed in the past for  $\text{H}_2\text{SO}_4\text{-H}_2\text{O}$  binary homogeneous nucleation  
80 (e.g., Vehkamäki et al., 2002),  $\text{H}_2\text{SO}_4\text{-H}_2\text{O}$  ion-induced nucleation (e.g., Hamill et al., 1982; Raes  
81 et al., 1986; Laakso et al., 2003), and  $\text{H}_2\text{SO}_4\text{-H}_2\text{O-NH}_3$  ternary homogeneous nucleation (Coffman  
82 and Hegg, 1995; Korhonen et al., 1999; Napari et al., 2002) have been based on the classical  
83 approach, which employs capillarity approximation (i.e., assuming that small clusters have same  
84 properties as bulk) and calculate nucleation rates according to the free energy change associated  
85 with the formation of a “critical embryo”. Yu and Turco (1997, 2000, 2001) developed a neutral  
86 and charged binary  $\text{H}_2\text{SO}_4\text{-H}_2\text{O}$  nucleation model using a kinetic approach that explicitly treats  
87 the complex interactions among small air ions, neutral and charged clusters of various sizes,  
88 precursor vapor molecules, and pre-existing aerosols. The formation and evolution of cluster size  
89 distributions for positively and negatively charged cluster ions and neutral clusters affected by  
90 ionization, recombination, neutralization, condensation, evaporation, coagulation, and scavenging,  
91 has been named as ion-mediated nucleation (IMN) (Yu and Turco, 2000). The IMN theory  
92 significantly differs from classical ion-induced nucleation (IIN) theory (e.g., Hamill et al., 1982;  
93 Raes et al., 1986; Laakso et al., 2003) which is based on a simple modification of the free energy  
94 for the formation of a “critical embryo” by including the electrostatic potential energy induced by  
95 the embedded charge (i.e., Thomson effect (Thomson, 1888)). The classical approach does not  
96 properly account for the kinetic limitation to embryo development, enhanced stability and growth  
97 of charged clusters associated with dipole-charge interaction (Nadykto and Yu, 2003; Yu, 2005),  
98 and the important contribution of neutral clusters resulting from ion-ion recombination to  
99 nucleation (Yu and Turco, 2011). In contrast, these important physical processes are explicitly  
100 considered in the kinetic-based IMN model (Yu, 2006b).



101 Since the beginning of the century, nucleation models based on kinetic approach have also  
102 been developed in a number of research groups (Lovejoy et al., 2004; Sorokin et al., 2006; Chen  
103 et al., 2012; Dawson et al., 2012; McGrath et al., 2012). Lovejoy et al. (2004) developed a kinetic  
104 ion nucleation model, which explicitly treats the evaporation of small neutral and negatively  
105 charged H<sub>2</sub>SO<sub>4</sub>-H<sub>2</sub>O clusters. The thermodynamic data used in their model were obtained from  
106 measurements of small ion clusters, ab initio calculations, thermodynamic cycle, and some  
107 approximations (adjustment of Gibbs free energy for neutral clusters calculated based on liquid  
108 droplet model, interpolation, etc.). Lovejoy et al. (2004) did not consider the nucleation on positive  
109 ions. Sorokin et al. (2006) developed an ion-cluster-aerosol kinetic (ICAK) model which uses the  
110 thermodynamic data reported in Froyd and Lovejoy (2003a, b) and empirical correction terms  
111 proposed by Lovejoy et al. (2004). Sorokin et al. (2006) used the ICAK model to simulate  
112 dynamics of neutral and charged H<sub>2</sub>SO<sub>4</sub>-H<sub>2</sub>O cluster formation and compared the modeling results  
113 with their laboratory measurements. Chen et al. (2012) developed an approach for modeling new  
114 particle formation based on a sequence of acid-base reactions, with sulfuric acid evaporation rates  
115 (from clusters) estimated empirically based on measurements of neutral molecular clusters taken  
116 in Mexico City and Atlanta. Dawson et al. (2012) presented a semi-empirical kinetics model for  
117 nucleation of methanesulfonic acid (MSA), amines, and water that explicitly accounted for the  
118 sequence of reactions leading to formation of stable particles. The kinetic models of Chen et al.  
119 (2012) and Dawson et al. (2012) consider only neutral clusters.

120 McGrath et al. (2012) developed the Atmospheric Cluster Dynamics Code (ACDC) to model  
121 the cluster kinetics by solving the birth–death equations explicitly, with evaporation rate  
122 coefficients derived from formation free energies calculated by quantum chemical methods  
123 (Almeida et al., 2013; Olenius et al., 2013). The ACDC model applied to the H<sub>2</sub>SO<sub>4</sub>-  
124 dimethylamine (DMA) system considers 0–4 base molecules and 0–4 sulfuric acid molecules  
125 (Almeida et al., 2013). Olenius et al. (2013) applied the ACDC model to simulate the steady-state  
126 concentrations and kinetics of neutral, and negatively and positively charged clusters containing  
127 up to 5 H<sub>2</sub>SO<sub>4</sub> and 5 NH<sub>3</sub> molecules. In ACDC, the nucleation rate is calculated as the rate of  
128 clusters growing larger than the upper bounds of the simulated system (i.e., clusters containing 4  
129 or 5 H<sub>2</sub>SO<sub>4</sub> molecules) (Kurten et al., 2016).

130 The kinetic IMN model developed by Yu and Turco (1997, 2001) explicitly simulates the  
131 dynamics of neutral, positively charged, and negatively charged clusters, based on a discrete-  
132 sectional bin structure that covers the clusters containing 0, 1, 2, ..., 15, ... H<sub>2</sub>SO<sub>4</sub> molecules to  
133 particles containing thousands of H<sub>2</sub>SO<sub>4</sub> (and H<sub>2</sub>O) molecules. In the first version of the kinetic  
134 IMN model (Yu and Turco, 1997, 2001), due to the lack of thermodynamic data for the small  
135 clusters, the compositions of neutral and charged clusters were assumed to be the same and the  
136 evaporation of small clusters was accounted for using a simple adjustment to the condensation

137 accommodation coefficients. Yu (2006b) developed a second-generation IMN model which  
138 incorporated newer thermodynamic data (Froyd, 2002; Wilhelm et al., 2004) and physical  
139 algorithms (Froyd, 2002; Wilhelm et al., 2004) and explicitly treated the evaporation of neutral  
140 and charged clusters. Yu (2007) further improved the IMN model by using two independent  
141 measurements (Marti et al., 1997; Hanson and Eisele, 2000) to constrain monomer hydration in  
142 the H<sub>2</sub>SO<sub>4</sub>-H<sub>2</sub>O system and by incorporating experimentally determined energetics of small  
143 neutral H<sub>2</sub>SO<sub>4</sub>-H<sub>2</sub>O clusters that became available then (Hanson and Lovejoy, 2006; Kazil et al.,  
144 2007). The first and second generations of the IMN model were developed for the H<sub>2</sub>SO<sub>4</sub>-H<sub>2</sub>O  
145 binary system, although the possible effects of ternary species such as the impact of NH<sub>3</sub> on the  
146 stability of both neutral and charged pre-nucleation clusters have been pointed out in these  
147 previous studies (Yu and Turco, 2001; Yu, 2006b). The present work extends the previous versions  
148 of the IMN model in binary H<sub>2</sub>SO<sub>4</sub>-H<sub>2</sub>O system to ternary H<sub>2</sub>SO<sub>4</sub>-H<sub>2</sub>O-NH<sub>3</sub> system, as described  
149 below.

150

## 151 2.2. Model representation of kinetic ternary nucleation processes

152 Figure 1 schematically illustrates the evolution of charged and neutral clusters/droplets  
153 explicitly simulated in the kinetic H<sub>2</sub>SO<sub>4</sub>-H<sub>2</sub>O-NH<sub>3</sub> TIMN model. Here, H<sub>2</sub>SO<sub>4</sub> (S) is the key  
154 atmospheric nucleation precursor driving the TIMN process while ions, H<sub>2</sub>O (W), and NH<sub>3</sub> (A)  
155 stabilize the H<sub>2</sub>SO<sub>4</sub> clusters and enhance in this way H<sub>2</sub>SO<sub>4</sub> nucleation rates. Ions also enhance  
156 cluster formation rates due to the interaction with polar nucleating species leading to enhanced  
157 collision cross sections (Nadykto and Yu, 2003). The airborne ions are generated by galactic  
158 cosmic rays (GCRs) or produced by radioactive emanations, lightning, corona discharge,  
159 combustion and other ionization sources. The initial negative ions, which are normally assumed to  
160 be NO<sub>3</sub><sup>-</sup>, are converted into HSO<sub>4</sub><sup>-</sup> core ions (i.e., S<sup>-</sup>) and, then, to larger H<sub>2</sub>SO<sub>4</sub> clusters in the

161 presence of gaseous H<sub>2</sub>SO<sub>4</sub>. The initial positive ions H<sup>+</sup>W<sub>w</sub> are converted into H<sup>+</sup>A<sub>1-2</sub>W<sub>w</sub> in the  
162 presence of NH<sub>3</sub>, H<sup>+</sup>S<sub>s</sub>W<sub>w</sub> in the presence of H<sub>2</sub>SO<sub>4</sub>, or H<sup>+</sup>A<sub>a</sub>S<sub>s</sub>W<sub>w</sub> in the case, when both NH<sub>3</sub>  
163 and H<sub>2</sub>SO<sub>4</sub> are present in the nucleating vapors. Some of the binary H<sub>2</sub>SO<sub>4</sub>-H<sub>2</sub>O clusters, both  
164 neutral and charged, transform into ternary ones by taking up NH<sub>3</sub> vapors. The molar fraction of  
165 ternary clusters in nucleating vapors depends on [NH<sub>3</sub>], the binding strength of NH<sub>3</sub> to binary and  
166 ternary pre-nucleation clusters, cluster composition, and ambient conditions such as T and RH.

167 Similar to the kinetic binary IMN (BIMN) model (Yu, 2006b), the kinetic TIMN model  
168 employs a discrete-sectional bin structure to represent clusters/particles. The bin index *i* represent  
169 the amount of core component (i.e., H<sub>2</sub>SO<sub>4</sub>). For small clusters ( $i \leq i_d = 30$  in this study), *i* is the

170 number of H<sub>2</sub>SO<sub>4</sub> molecules in the cluster (i.e.,  $i = s$ ) and the core volume of  $i^{\text{th}}$  bin  $v_i = i \times v_l$ , where  
 171  $v_l$  is the volume of one H<sub>2</sub>SO<sub>4</sub> molecule. When  $i > i_d$ ,  $v_i = VRAT_i \times v_{i-1}$ , where  $VRAT_i$  is the volume  
 172 ratio of  $i^{\text{th}}$  bin to  $(i-1)^{\text{th}}$  bin. The discrete-sectional bin structure enables the model to cover a wide  
 173 range of sizes of nucleating clusters/particles with the highest possible size resolution for small  
 174 clusters (Yu, 2006b). For clusters with a given bin  $i$ , the associated amounts of water and NH<sub>3</sub> and  
 175 thus the effective radius of each ternary cluster are calculated based on the equilibrium of  
 176 clusters/particles with the water vapor and/or ammonia, as described in later sections.

177 The evolution of positive, negative, and neutral clusters due to the simultaneous condensation,  
 178 evaporation, recombination, coagulation, and other loss processes, is described by the following  
 179 differential equations obtained by the modification of those describing for the evolution of binary  
 180 H<sub>2</sub>SO<sub>4</sub>-H<sub>2</sub>O system (Yu, 2006b):

$$181 \quad \frac{\partial N_0^+}{\partial t} = Q + \gamma_1^+ N_1^+ - N_0^+ \left( \sum_{j=1}^{i_{\max}} \beta_{i,j}^+ N_j^0 + \sum_{j=0}^{i_{\max}} \eta_{i,j}^+ N_j^+ + \sum_{j=0}^{i_{\max}} \alpha_{0,j}^{+,-} N_j^- \right) - N_0^+ L_0^+ \quad (1)$$

$$182 \quad \frac{\partial N_0^-}{\partial t} = Q + \gamma_1^- N_1^- - N_0^- \left( \sum_{j=1}^{i_{\max}} \beta_{i,j}^- N_j^0 + \sum_{j=0}^{i_{\max}} \eta_{i,j}^- N_j^- + \sum_{j=0}^{i_{\max}} \alpha_{0,j}^{-,+} N_j^+ \right) - N_0^- L_0^- \quad (2)$$

$$183 \quad \frac{\partial N_1^0}{\partial t} = P_{\text{H}_2\text{SO}_4} + \sum_{j=2}^{i_{\max}} \delta_{j,2} \gamma_j^0 N_j^0 + \sum_{j=1}^{i_{\max}} (\gamma_j^+ N_j^+ + \gamma_j^- N_j^-) - N_1^0 \left( \sum_{j=1}^{i_{\max}} (1 - f_{1,j,1}) \beta_{1,j}^0 N_j^0 + \sum_{j=0}^{i_{\max}} (\beta_{j,1}^+ N_j^+ + \beta_{j,1}^- N_j^-) \right) - N_1^0 L_1^0 \quad (3)$$

$$184 \quad \frac{\partial N_i^+(i \geq 1)}{\partial t} = g_{i+1,i} \gamma_{i+1}^+ N_{i+1}^+ - g_{i,i-1} \gamma_i^+ N_i^+ + \sum_{j=0}^{i-1} \sum_{k=1}^i \frac{v_j}{v_i} f_{j,k,i} \beta_{j,k}^+ N_j^+ N_k^0 + \sum_{j=0}^{i-1} \sum_{k=0}^i \frac{v_j}{v_i} f_{j,k,i} \eta_{j,k}^+ N_j^+ N_k^+ + \sum_{j=0}^i \sum_{k=1}^i \frac{v_k}{v_i} f_{j,k,i} \beta_{j,k}^+ N_j^+ N_k^0 - N_i^+ \left( \sum_{j=1}^{i_{\max}} (1 - f_{i,j,i}) \beta_{i,j}^+ N_j^0 + \sum_{j=0}^{i_{\max}} (1 - f_{i,j,i}) \eta_{i,j}^+ N_j^+ + \sum_{j=0}^{i_{\max}} \alpha_{i,j}^{+,-} N_j^- \right) - N_i^+ L_i^+ \quad (4)$$

$$185 \quad \frac{\partial N_i^-(i \geq 1)}{\partial t} = g_{i+1,i} \gamma_{i+1}^- N_{i+1}^- - g_{i,i-1} \gamma_i^- N_i^- + \sum_{j=0}^{i-1} \sum_{k=1}^i \frac{v_j}{v_i} f_{j,k,i} \beta_{j,k}^- N_j^- N_k^0 + \sum_{j=0}^{i-1} \sum_{k=0}^i \frac{v_j}{v_i} f_{j,k,i} \eta_{j,k}^- N_j^- N_k^- + \sum_{j=0}^i \sum_{k=1}^i \frac{v_k}{v_i} f_{j,k,i} \beta_{j,k}^- N_j^- N_k^0 - N_i^- \left( \sum_{j=1}^{i_{\max}} (1 - f_{i,j,i}) \beta_{i,j}^- N_j^0 + \sum_{j=0}^{i_{\max}} (1 - f_{i,j,i}) \eta_{i,j}^- N_j^- + \sum_{j=0}^{i_{\max}} \alpha_{i,j}^{-,+} N_j^+ \right) - N_i^- L_i^- \quad (5)$$

$$186 \quad \frac{\partial N_i^0(i \geq 2)}{\partial t} = g_{i+1,i} \gamma_{i+1}^0 N_{i+1}^0 - g_{i,i-1} \gamma_i^0 N_i^0 + \sum_{j=lk=1}^{i-1} \sum_{k=1}^{i-1} \frac{v_k}{v_i} f_{j,k,i} \beta_{j,k}^0 N_j^0 N_k^0 + \sum_{j=0}^i \sum_{k=0}^i f_{j,k,i} \alpha_{j,k}^{+,-} \left( \frac{v_k}{v_i} N_j^+ N_k^- + \frac{v_j}{v_i} N_j^- N_k^+ \right) - N_i^0 \left( \sum_{j=1}^{i_{\max}} (1 - f_{i,j,i}) \beta_{i,j}^0 N_j^0 + \sum_{j=0}^{i_{\max}} (\beta_{j,i}^+ N_j^+ + \beta_{j,i}^- N_j^-) \right) - N_i^0 L_i^0 \quad (6)$$

187

188 In Eqs. (1-6), the superscripts “+”, “-”, and “0” refer to positive, negative, and neutral clusters,  
189 respectively, while subscripts  $i, j, k$  represent the bin indexes.  $N_0^{+,-}$  and  $Q$  are the concentration of  
190 initial ions not containing  $\text{H}_2\text{SO}_4$  (i.e.,  $\text{H}^+\text{A}_a\text{W}_w$  and  $\text{NO}_3^-$ ) and the ionization rate, respectively.  $N_i$   
191 is the total number concentration ( $\text{cm}^{-3}$ ) of all cluster/particles (binary + ternary) in the bin  $i$ . For  
192 small clusters ( $i \leq i_d$ ),  $N_i$  is the number concentration ( $\text{cm}^{-3}$ ) of all clusters containing  $i$   $\text{H}_2\text{SO}_4$   
193 molecules. For example,  $N_1^0$  is the total concentration of binary and ternary neutral clusters  
194 containing one  $\text{H}_2\text{SO}_4$  molecules. Index  $i$  in Eq. (5) refers to the sum of  $\text{H}_2\text{SO}_4$  and  $\text{HSO}_4^-$ . The  
195 second term of Eq. (2) describes the reaction of  $\text{HSO}_4^- + \text{HNO}_3 \rightarrow \text{NO}_3^- + \text{H}_2\text{SO}_4$ . Although the  
196 rate of this reaction is generally negligible, we keep the term there for completeness.  $P_{\text{H}_2\text{SO}_4}$  is the  
197 gas-phase production rate of neutral  $\text{H}_2\text{SO}_4$  molecules.  $L_i^{+,-,0}$  is the loss rate due to scavenging by  
198 pre-existing particles, and wall and dilution losses in the laboratory chamber studies (Kirkby et al.,  
199 2011; Olenius et al., 2013; Kurten et al., 2016).  $f_{j,k,i}$  is the volume fraction of intermediate particles  
200 (volume =  $v_j + v_k$ ) partitioned into bin  $i$  with respect to the core component –  $\text{H}_2\text{SO}_4$ , as defined in  
201 Jacobson et al. (1994).  $g_{i+1,i} = v_1 / (v_{i+1} - v_i)$  is the volume fraction of intermediate particles of  
202 volume ( $v_{i+1} - v_1$ ) partitioned into bin  $i$ .  $\delta_{j,2} = 2$  at  $j=2$  and  $\delta_{j,2} = 1$  at  $j \neq 2$ .  $\gamma_i^+, \gamma_i^-,$  and  $\gamma_i^0$  are the  
203 mean (or effective) cluster evaporation coefficients for positive, negative and neutral clusters in  
204 bin  $i$ , respectively.  $\beta_{i,j}^+, \beta_{i,j}^-, \beta_{i,j}^0$  are the coagulation kernels for the neutral clusters/particles in  
205 bin  $j$  interacting with positive, negative, and neutral clusters/particles in bin  $i$ , respectively, which  
206 reduce to the condensation coefficients for  $\text{H}_2\text{SO}_4$  monomers at  $j=1$ .  $\eta_{j,k}^+$  and  $\eta_{j,k}^-$  are  
207 coagulation kernels for clusters/particles of like sign from bin  $j$  and clusters/particles from bin  $k$ .  
208 It should be noted that the electrostatic repulsion is too strong for small clusters to gain more than  
209 one charge. However, small charged clusters can be scavenged by large pre-existing particles of  
210 same polarity. Large pre-existing particles serve as the sink for small clusters in the model and the  
211 effect of multiple charge is small and thus is not tracked.  $\alpha_{i,j}^{+,-}$  is the recombination coefficient  
212 for positive clusters/particles in bin  $i$  interacting with negative clusters/particles in bin  $j$ , while  
213  $\alpha_{i,j}^{-,+}$  is the recombination coefficient negative clusters/particles from bin  $i$  interacting with  
214 positively charged clusters/particles from bin  $j$ .

215 The methods for calculating  $\beta$ ,  $\gamma$ ,  $\eta$ , and  $\alpha$  for binary H<sub>2</sub>SO<sub>4</sub>-H<sub>2</sub>O clusters have been described  
 216 in our previous publications (Yu and Turco, 2001; Nadykto and Yu, 2003; Yu, 2006b). Dipole-  
 217 charge interaction (Nadykto and Yu, 2003), image capture and three-body trapping effects (Hoppel  
 218 and Frick, 1986) are considered in the calculation of these coefficients. Since  $\beta$ ,  $\eta$ , and  $\alpha$  depend  
 219 on the cluster mass (or size) rather than on the cluster composition, schemes for calculating these  
 220 properties in binary and ternary clusters are identical. In contrast,  $\gamma$  is quite sensitive to cluster  
 221 composition. The evaporation rate coefficient of H<sub>2</sub>SO<sub>4</sub> molecules from clusters containing  $i$   
 222 H<sub>2</sub>SO<sub>4</sub> molecules ( $\gamma_i$ ) is largely controlled by the stepwise Gibbs free energy change  $\Delta G_{i-1,i}$  of  
 223 formation of an  $i$ -mer from an  $(i-1)$ -mer (Yu, 2007)

$$224 \quad \gamma_i = \beta_{i-1} N^0 \exp\left(\frac{\Delta G_{i-1,i}}{RT}\right) \quad (7)$$

$$225 \quad \Delta G_{k-1,k} = -RT \ln\left(\frac{N_{\pm}^0}{N^0}\right) \pm \Delta H_{k-1,k}^0 - T\Delta S_{k-1,k}^0 \quad (8)$$

226 where  $R$  is the molar gas constant,  $N^0$  is the arbitrary number concentration of a hypothetical gas  
 227 consisting solely of the species for which the calculation is performed (generally number  
 228 concentration of H<sub>2</sub>SO<sub>4</sub> at a given T under the reference vapor pressure  $P$  of 1 atm).  $\Delta H^0$  and  $\Delta S^0$   
 229 are enthalpy and entropy changes under the standard conditions (T=298 K, P=1 atm), respectively.  
 230 The temperature dependence of  $\Delta H^0$  and  $\Delta S^0$ , which is generally small and typically negligible  
 231 over the temperature range of interest (Nadykto et al., 2009), was not considered.

### 233 2.3. Thermochemical data of neutral and charged binary and ternary clusters

234  $\Delta H$ ,  $\Delta S$  and  $\Delta G$  values needed to calculate cluster evaporation rates (Eq. 7) for the TIMN  
 235 model can be derived from laboratory measurements and computational quantum chemistry (QC)  
 236 calculation. Thermochemical properties of neutral and charged binary and ternary clusters  
 237 obtained using the computational chemical methods and comparisons of computed energies with  
 238 available experimental data and semi-experimental estimates are given in Tables A1-A4 and  
 239 discussed in Appendix. As an example, Figure 2 shows  $\Delta G$  associated with the addition of water  
 240 ( $\Delta G_{+W}^0$ ), ammonia ( $\Delta G_{+A}^0$ ), and sulfuric acid ( $\Delta G_{+S}^0$ ) to binary and ternary clusters as a function of  
 241 the cluster hydration number  $w$ . H<sub>2</sub>O has high proton affinity and, thus, H<sub>2</sub>O is strongly bonded to  
 242 all positive ions with low  $w$ .  $\Delta G_{+W}^0$  expectedly becomes less negative and binding of H<sub>2</sub>O to binary  
 243 and ternary clusters weakens due to the screening effect as the hydration number  $w$  is growing  
 244 (Fig. 2a). The presence of NH<sub>3</sub> in the clusters weakens binding of H<sub>2</sub>O to positive ions. For

245 example,  $\Delta G_{+W}^0$  for  $H^+A_1W_wS_1$  is  $\sim 3-4$  kcal mol<sup>-1</sup> less negative than that for  $H^+W_wS_1$  at  $w=3-6$ .  
246 The addition of one more  $NH_3$  to the clusters to form  $H^+A_2W_w$  and  $H^+A_2W_wS_1$  further weakens  
247  $H_2O$  binding by  $\sim 1.5-6$  kcal mol<sup>-1</sup> at  $w=1-3$ , while exhibiting much smaller impact on hydration  
248 free energies at  $w>3$ . Both the absolute values and trends in  $\Delta G_{+W}^0$  derived from calculations are  
249 in agreement with the laboratory measurements within the uncertainty range of  $\sim 1-2$  kcal mol<sup>-1</sup> for  
250 both QC calculations and measurements. This confirms the efficiency and precision of QC  
251 methods in calculating thermodynamic data needed for the development of nucleation models.

252 The proton affinity of  $NH_3$  is 204.1 kcal mol<sup>-1</sup>, which is 37.5 kcal mol<sup>-1</sup> higher than that of  
253  $H_2O$  (166.6 kcal mol<sup>-1</sup>) (Jolly, 1991). The hydrated hydronium ions ( $H^+W_w$ ) are easily converted  
254 to  $H^+A_1W_w$  in the presence of  $NH_3$ . The binding of  $NH_3$  and  $H_2O$  molecule to  $H^+W_w$  exhibits a  
255 similar pattern. In particular, binding of  $NH_3$  to  $H^+W_w$  decreases as  $w$  is growing, with  $\Delta G_{+A}^0$  for  
256  $H^+A_1W_w$  ranging from -52.08 kcal mol<sup>-1</sup> at  $w=1$  to -8.32 kcal mol<sup>-1</sup> at  $w=9$ . The binding of  $NH_3$   
257 to  $H^+W_wS_1$  ions is also quite strong, with  $\Delta G_{+A}^0$  for  $H^+A_1W_wS_1$  ranging from -33.14 kcal mol<sup>-1</sup> at  
258  $w=1$  and to -10.57 kcal mol<sup>-1</sup> at  $w=6$ . The addition of the  $NH_3$  molecule to  $H^+A_1W_w$  (to form  
259  $H^+A_2W_w$ ) is much less favorable thermodynamically than that to  $H^+W_w$ , with the corresponding  
260  $\Delta G_{+A}^0$  being -22 kcal mol<sup>-1</sup> and -6 kcal mol<sup>-1</sup> at  $w=2$  and  $w=6$ , respectively. The  $\Delta G_{+A}^0$  values for  
261  $H^+A_2W_w$  are 3-5 kcal mol<sup>-1</sup> more negative than the experimental values at  $w=0-1$ ; however, they  
262 are pretty close to experimental data at  $w=2-3$  (Fig. 2b and Table A2). While it is possible that the  
263 QC method overestimates the charge effect on the formation free energies of smallest clusters, the  
264 possible overestimation at  $w=0-1$  will not affect nucleation calculations because most of  $H^+A_2W_w$   
265 in the atmosphere contain more than 2 water molecules (i.e.,  $w>2$ ) due to the strong hydration (see  
266 Table A2 and Fig. 2a).

267 A comparison of QC and semi-experimental estimates of  $\Delta G_{+S}^0$  values associated with the  
268 attachment of  $H_2SO_4$  to positive ions shown in Fig. 2c indicates that computed  $\Delta G_{+S}^0$  values agree  
269 well with observations for  $H^+W_wS_1$  and  $H^+A_1W_wS_1$  but differ by  $\sim 2-4$  kcal mol<sup>-1</sup> from semi-  
270 experimental values for  $H^+A_2W_wS_1$ . As seen from Figs. 2a and 2c, the attachment of  $NH_3$  to  
271  $H^+W_wS_1$  weakens the binding of both  $H_2O$  and  $H_2SO_4$  to the clusters. This suggests that the  
272 attachment of  $NH_3$  leads to the evaporation of  $H_2SO_4$  and  $H_2O$  molecules from the clusters. In  
273 other words,  $H_2SO_4$  is less stable in  $H^+A_1W_wS_1$  than in  $H^+W_wS_1$  (Fig. 2c). While this may be taken  
274 for the indication that  $NH_3$  inhibits nucleation on positive ions at the first look, further calculations  
275 show that binding of  $NH_3$  to  $H^+A_1W_wS_1$  is quite strong (Fig. 2b) and that  $H_2SO_4$  in  $H^+A_2W_wS_1$   
276 cluster is much more stable than that in  $H^+A_1W_wS_1$ , with  $\Delta G_{+S}^0$  being by  $\sim 7$  kcal mol<sup>-1</sup> more  
277 negative at  $w>2$ . The  $H^+A_2W_wS_1$  cluster can also be formed via the attachment of  $H_2SO_4$  to  
278  $H^+A_2W_w$ . In the presence of sufficient concentrations of  $NH_3$ , a large fraction of positively charged  
279  $H_2SO_4$  monomers exist in the form of  $H^+A_2W_wS_1$  and, hence,  $NH_3$  enhances nucleation of positive  
280 ions. Since positively charged  $H_2SO_4$  dimers are expected to contain large number of water

281 molecules, we have not yet computed and derived quantum chemical data for these clusters. The  
282 CLOUD measurements do indicate that once  $H^+A_2W_wS_1$  are formed, they can continue to grow  
283 to larger  $H^+A_aW_wS_s$  clusters along  $a=s+1$  pathway (Schobesberger et al., 2015).

284 Figure 2 shows clearly that the calculated values in most cases agree with measurements within  
285 the uncertainty range that justifies the application of QC values in the case, when no reliable  
286 experimental data are available.

287

## 288 2.4. Nucleation barriers for neutral/charged clusters and size-dependent evaporation rates

289 Nucleation barriers and cluster evaporation rates are critically important for calculations of  
290 nucleation rates. This section describes the methods employed to calculate the evaporation rates  
291 of nucleating clusters of variable sizes and compositions (i.e.,  $\gamma$  in Eqs. 1-6) in the TIMN model.

292

### 293 2.4.1 Equilibrium distributions of small binary and ternary clusters

294 In the atmosphere,  $[H_2O]$  is much higher than  $[H_2SO_4]$  and, thus,  $H_2SO_4$  clusters/particles are  
295 always in equilibrium with water vapor (Yu, 2007). In the lower troposphere, where most of the  
296 nucleation events were observed,  $[H_2SO_4]$  is typically at sub-ppt to ppt level, while  $[NH_3]$  is in the  
297 range of sub-ppb to ppb levels (Butler et al., 2016; Warner et al., 2016) (note that, in what follows,  
298 all references to vapor mixing ratios – parts per billion and parts per trillion – are by volume). This  
299 means that small ternary clusters can be considered to be in equilibrium with  $H_2O$  and  $NH_3$  vapors.  
300 Like the previous BIMN model derived assuming equilibrium of binary clusters with water vapor,  
301 the present TIMN model treats small clusters containing a given number of  $H_2SO_4$  molecules as  
302 being in equilibrium with both  $H_2O$  and  $NH_3$ . Their relative concentrations are calculated using  
303 the thermodynamic data shown in Tables A1-A4. It should be noted that the system may deviate  
304 from equilibrium and the model scheme is probably not suitable if when  $[NH_3]$  is less than or close  
305 to  $[H_2SO_4]$ . Under such cases, the equilibrium assumption may overestimate nucleation rates.

306 Figure 3 shows the relative abundance (or molar fractions) of small positive, negative, and  
307 neutral clusters ( $f_{s,a,w}^{+,-,0}$ ) containing a given number of  $H_2SO_4$  molecules at the ambient temperature  
308 of 292 K and three different combinations of RH and  $[NH_3]$  values. As a result of relative  
309 instability of  $H_2SO_4$  in  $H^+A_1W_wS_1$  compared to  $H^+W_wS_1$  or  $H^+A_2W_wS_1$  (Fig. 2c), most of positive  
310 ions with one  $H_2SO_4$  molecule exist in the form of either as  $H^+W_wS_1$  or  $H^+A_2W_wS_1$  (i.e, containing  
311 either zero or two  $NH_3$  molecules, Fig. 3a). When  $[NH_3]=0.3$  ppb (with  $T=292$  K), most of the  
312 positive ions containing one  $H_2SO_4$  molecule do not contain  $NH_3$  and their composition is  
313 dominated by  $H^+W_wS_1$  ( $\bar{w} \approx 7$ ). At the given T and  $[NH_3]=0.3$  ppb, around 17% of positive ions  
314 with one  $H_2SO_4$  molecule contain two  $NH_3$  molecules at RH=38%. The fraction of positive ions  
315 containing one  $H_2SO_4$  and two  $NH_3$  molecules decreases to 0.9%, when RH = 90%. At T=292 K  
316 and RH=38%, the increase in  $[NH_3]$  by a factor of 10 to 3 ppb leads to the domination of

317  $\text{H}^+\text{A}_2\text{W}_w\text{S}_1$  (~95%) in the composition of positively charged  $\text{H}_2\text{SO}_4$  monomers. As expected, the  
318 composition of positive ions and their contribution to nucleation depends on T, RH, and  $[\text{NH}_3]$ .  
319 The incorporation of the quantum chemical and experimental clustering thermodynamics in the  
320 framework of the kinetic nucleation model enables us to study all these dependencies.

321 As a result of very weak binding of  $\text{H}_2\text{O}$  and  $\text{NH}_3$  to small negative ions (Table A4), nearly all  
322 negatively charged clusters with  $s=0-1$  do not contain water and ammonia (not shown). In the case,  
323 when  $s$  is growing to 2, all  $\text{S}^-\text{S}_2\text{A}_a\text{W}_w$  clusters still do not contain  $\text{NH}_3$  (i.e.,  $a=0$ ), while only 20-  
324 40% of them contain one water molecule ( $w=1$ ) (Fig. 3b). As  $s$  further increases to 3,  $\text{NH}_3$  begins  
325 to get into some of the negatively charged ions. The fraction of  $\text{S}^-\text{S}_3\text{A}_a\text{W}_w$  clusters containing one  
326  $\text{NH}_3$  molecule is 9% at  $\text{RH}=38\%$  and  $[\text{NH}_3]=0.3\text{ppb}$ , 3% at  $\text{RH}=90\%$  and  $[\text{NH}_3]=0.3\text{ppb}$ , and  
327 50% at  $\text{RH}=38\%$  and  $[\text{NH}_3]=3\text{ppb}$ . Most of  $\text{S}^-\text{S}_3\text{W}_w$  clusters are hydrated while the fraction of  $\text{S}^-\text{S}_3\text{A}_a\text{W}_w$   
328 clusters containing two  $\text{NH}_3$  molecules at these ambient conditions is negligible. The  
329 fraction of negative cluster ions containing two  $\text{NH}_3$  molecules becomes significant at  $s=4$  (Fig.  
330 3b) and increases from 28% at  $[\text{NH}_3]=0.3\text{ppb}$  to 80% at  $[\text{NH}_3]=3\text{ppb}$  at  $\text{RH}=38\%$ . At  $[\text{NH}_3]=0.3$   
331  $\text{ppb}$ , the increase in RH from 38% to 90% reduces the fraction of  $\text{NH}_3$  containing  $\text{S}^-\text{S}_3\text{A}_a\text{W}_w$   
332 clusters (i.e.,  $a \geq 1$ ) from 95% to 70%, demonstrating a significant impact of RH on cluster  
333 compositions and emphasizing the importance of accounting for the RH in calculations of ternary  
334 nucleation rates.

335 The equilibrium distributions of neutral clusters are presented in Fig. 3c ( $\text{H}_2\text{SO}_4$  monomers  
336 and dimers) and Fig. 3d ( $\text{H}_2\text{SO}_4$  trimers and tetramers). Hydration is accounted for in the case of  
337 monomers and dimers and not included, due to lack of thermodynamic data, in calculations for  
338 trimers and tetramers. Based on the thermodynamic data shown in Table A3, the dominant fraction  
339 of neutral monomers is hydrated (79% at  $\text{RH}=38\%$  and 94% at  $\text{RH}=90\%$ ) while the fraction of  
340 monomers containing  $\text{NH}_3$  is negligible (0.02% at  $[\text{NH}_3]=0.3\text{ppb}$  and 0.2% at  $[\text{NH}_3]=3\text{ppb}$ ,  
341  $\text{RH}=38\%$ ). As a result of the growing binding strength of  $\text{NH}_3$  with the cluster size (Table A3),  
342 the fraction of neutral sulfuric acid dimers containing one  $\text{NH}_3$  molecule reaches 18% at  
343  $[\text{NH}_3]=0.3\text{ppb}$  and 69% at  $[\text{NH}_3]=3\text{ppb}$  when  $T=292\text{K}$  and  $\text{RH}=38\%$ . In the case of  $\text{H}_2\text{SO}_4$   
344 trimers and tetramers, data shown in Figure 3d are limited to the relative abundance of unhydrated  
345 clusters only. Under the given conditions, most of trimers contain two  $\text{NH}_3$  molecules while most  
346 tetramers contain 3  $\text{NH}_3$  molecules. At  $[\text{NH}_3]=3\text{ppb}$ , ~2% of trimers contain three  $\text{NH}_3$  molecules  
347 (i.e.,  $s=a=3$ ) and 55% of tetramers contain four  $\text{NH}_3$  molecules (i.e.,  $s=a=4$ ). As a result of a  
348 significant drop of  $\Delta G_{+A}^0$  in the case, when  $a/s$  ratio exceeds one (Table A3), the fraction of neutral  
349 clusters with  $a=s+1$  are negligible. The cluster distributions clearly indicate that small sulfuric acid  
350 clusters are still not fully neutralized by  $\text{NH}_3$  even if  $[\text{NH}_3]$  is at  $\text{ppb}$  level; and that the degree of  
351 neutralization (i.e.,  $a:s$  ratio) increases with the cluster size.

352



353 2.4.2 Mean stepwise and accumulative Gibbs free energy change and impact of ammonia

354 In the TIMN model, the equilibrium distributions are used to calculate number concentrations  
 355 weighted stepwise Gibbs free energy change for adding one H<sub>2</sub>SO<sub>4</sub> molecule to form a neutral,  
 356 positively charged, and negatively charged cluster containing  $s$  H<sub>2</sub>SO<sub>4</sub> molecules ( $\overline{\Delta G}_{s-1,s}$ ):

$$357 \quad \overline{\Delta G}_{s-1,s}^{+,-,0} = \sum_{a,w} f_{s,a,w}^{+,-,0} \Delta G_{s-1,s,a,w}^{+,-,0} \quad (9)$$

358 where  $f_{s,a,w}^{+,-,0}$  is the equilibrium fraction of a particular cluster within a cluster type as shown in  
 359 Fig. 3.

360 In the atmosphere, where substantial nucleation is observed, the sizes of critical clusters are  
 361 generally small ( $s < \sim 5-10$ ) (e.g., Sipilä et al., 2010) and nucleation rates are largely controlled by  
 362 the stability (or  $\gamma$ ) of small clusters with  $s < \sim 5-10$ . QC calculations and experimental data on  
 363 clustering thermodynamics available for clusters of small sizes (Tables A2–A4), are critically  
 364 important as the formation of these small clusters is generally the limiting step for nucleation.  
 365 Nevertheless, thermodynamics data for larger clusters are also needed to develop a robust  
 366 nucleation model that can calculate nucleation rates under various conditions. Both measurements  
 367 and QC calculations (Tables A2–A4) show significant effects of charge and charge signs (i.e.,  
 368 positive or negative) on the stability and composition of small clusters. These charge effects  
 369 decrease quickly as the clusters grow, due to the short-ranged nature of dipole-charge interaction  
 370 and the quick decrease of electrical field strength around charged clusters as cluster sizes increase  
 371 (Yu, 2005). Based on experimental data (Kearle et al., 1967; Davidson et al., 1977; Wlodek et  
 372 al., 1980; Holland and Castleman, 1982; Froyd and Lovejoy, 2003), the stepwise  $\Delta G$  values for  
 373 clusters decreases exponentially as the cluster sizes increase and approaches to the bulk values  
 374 when clusters containing more than  $\sim 8-10$  molecules (Yu, 2005). Cluster compositions measured  
 375 with an atmospheric pressure interface time-of-flight (APi-TOF) mass spectrometer during  
 376 CLOUD experiments also show that the difference in the composition of positively and negatively  
 377 charged clusters quickly decreases as the number of H<sub>2</sub>SO<sub>4</sub> molecules increases from 1 to  $\sim 10$  and  
 378 exhibits little further changes (Schobesberger et al., 2015).

379 In the present TIMN model, we assume that both neutral and charged clusters have the same  
 380 composition when  $s \geq 10$  and the following extrapolation scheme is used to calculate  $\Delta G_{s-1,s}$  for  
 381 clusters up to  $s=10$ :

$$382 \quad \Delta G_{s-1,s} = \Delta G_{s_1-1,s_1} + \frac{\left( \Delta G_{s_2-1,s_2} - \Delta G_{s_1-1,s_1} \right) \left( e^{-s_2 c} - e^{-s_1 c} \right)}{\left( e^{-s_2 c} - e^{-s_1 c} \right)} \quad (10)$$

383 where  $\Delta G_{s_1-1,s_1}$  is the stepwise mean Gibbs free energy change for H<sub>2</sub>SO<sub>4</sub> addition for a specific  
384 type (neutral, positive, or negative) of clusters at  $s=s_1$  that can be derived from QC calculation  
385 and/or experimental measurements, and  $\Delta G_{s_2-1,s_2}$  is the corresponding value for clusters at  $s=s_2$   
386 ( $=10$  in the present study) that is calculated in the capillarity approximation accounting for the  
387 Kelvin effect.  $c$  in Eq. 10 is the exponential coefficient that determines how fast  $\Delta G_{s-1,s}$   
388 approaches to bulk values as  $s$  increases. In the present study,  $c$  is estimated ~~by fitting from~~  $\Delta G_{s-1,s}$   
389 at  $s=2$  and  $s=3$  ~~based on Eq. (10) to for neutral binary and ternary clusters for which those from~~  
390 experimental (Hanson and Lovejoy, 2006; Kazil et al., 2007) or quantum-chemical data (Table  
391 A3) ~~are available~~. Apparently the interpolation approximation Eq. (10) is subject to uncertainty.  
392 Nevertheless, it is a reasonable approach to connect thermochemical properties of QC data for  
393 small binary and ternary clusters that cannot be adequately described by the capillarity  
394 approximation with those for large clusters that can be adequately described the very same  
395 capillarity approximation, and is the best approach we can come up with at this point in order to  
396 develop a model that can be applied to all conditions. Further QC and experimental studies of the  
397 thermodynamics of relatively larger clusters can help to reduce the uncertainty.

398 For clusters with  $s \geq s_2$ , the capillarity approximation is used to calculate  $\Delta G_{s-1,s}$  as

$$399 \quad \Delta G_{s-1,s} = -RT \ln(P/P_s) + \frac{2\sigma v_1 N_A}{r_s} \quad (11)$$

400 where  $P$  is the H<sub>2</sub>SO<sub>4</sub> vapor pressure and  $P_s$  is the H<sub>2</sub>SO<sub>4</sub> saturation vapor pressure over a flat  
401 surface with the same composition as the cluster.  $\sigma$  is the surface tension and  $v_1$  is the volume of  
402 one H<sub>2</sub>SO<sub>4</sub> molecule.  $r_s$  is the radius of the cluster and  $N_A$  is the Avogadro's number.

403 The scheme to calculate bulk  $\Delta G_{s-1,s}$  ( $s \geq 10$ ) for H<sub>2</sub>SO<sub>4</sub>-H<sub>2</sub>O binary clusters has been  
404 described in Yu (2007). For ternary nucleation, both experiments (Schobesberger et al., 2015) and  
405 QC calculations (Table A4) indicate that the growth of relatively large clusters follows the  $s=a$   
406 line (i.e, in the composition of ammonia bisulfate). In the present TIMN model, the bulk  $\Delta G_{s-1,s}$   
407 values for ternary clusters are calculated based on parameterized H<sub>2</sub>SO<sub>4</sub> saturation vapor pressure  
408 over ammonia bisulfate as a function of temperature, derived by Martin et al. (1997) from vapor  
409 pressures measured at temperature between 27 °C and °60 C, and surface tension measured at 298  
410 K from Hyvarinen et al. (2005). The uncertainty in saturation vapor pressures and surface tension

411 used in the calculation of the bulk  $\Delta G_{s-1,s}$  values is another source of uncertainty in the TIMN  
412 model, although it is likely to be small compared to other uncertainties as the nucleation is  
413 generally limited by the formation of small clusters.

414 Figure 4 presents stepwise ( $\overline{\Delta G_{s-1,s}}$ ) and cumulative (total)  $\overline{\Delta G_s}$  Gibbs free energy changes  
415 associated with the formation of neutral, positively charged, and negatively charged binary and  
416 ternary clusters containing  $s$   $\text{H}_2\text{SO}_4$  molecules under the conditions specified in the figure caption.  
417 The clusters are assumed to be in equilibrium with water (Yu, 2007) and ammonia (Fig. 3). As  
418 seen from Fig. 4, the presence of  $\text{NH}_3$  reduces the mean  $\overline{\Delta G_{s-1,s}}$  for larger clusters, which can be  
419 treated as the bulk binary  $\text{H}_2\text{SO}_4$ - $\text{H}_2\text{O}$  solution (Schobesberger et al., 2015), by  $\sim 3 \text{ kcal mol}^{-1}$ ,  
420 indicating a substantial reduction in the  $\text{H}_2\text{SO}_4$  vapor pressure over ternary solutions (Marti et al.,  
421 1997). The comparison also shows that the influence of  $\text{NH}_3$  on  $\overline{\Delta G_{s-1,s}}$  of small clusters ( $s \leq \sim 4$ )  
422 is much lower than that on larger ones and bulk solutions. For example, at  $[\text{NH}_3]=0.3 \text{ ppb}$ , the  
423 differences in  $\overline{\Delta G_{s-1,s}}$  between binary and ternary positive ions with  $s=1$  and neutral clusters with  
424  $s=2$  are only  $0.45 \text{ kcal mol}^{-1}$  and  $\sim 1 \text{ kcal mol}^{-1}$ , respectively. In the case of negative ions, zero  
425 and  $0.27\text{--}0.45 \text{ kcal mol}^{-1}$  differences at  $s \leq 2$  and  $s=3\text{--}4$ , respectively, were observed. The reduced  
426 effect of ammonia on smaller clusters is explained (Tables A2-A4) by ammonia's weaker bonding  
427 to smaller clusters than to larger ones, which in turn yields lower average  $\text{NH}_3$  to  $\text{H}_2\text{SO}_4$  ratios  
428 (Fig. 3). It should be noted that QC data for positively charged clusters are very limited and the  
429 interpolation approximation is subject to large uncertainty. In order for the nucleation on positive  
430 ions to occur, the first step is for  $\text{H}_2\text{SO}_4$  to attach to a positive ion that does not contain  $\text{H}_2\text{SO}_4$ .  
431 Unlike negative ions, the effect of charge on the bonding of  $\text{H}_2\text{SO}_4$  with positive ions is much  
432 weaker and thus the stepwise Gibbs free energy change for the addition of one  $\text{H}_2\text{SO}_4$  molecule to  
433 form a positively charged cluster is likely to be similar to that of neutral clusters, i.e., decreasing  
434 with cluster size. Therefore, the QC data for positively charged clusters containing one  $\text{H}_2\text{SO}_4$   
435 molecule provides a critical constrain. The success of the model in predicting the  $[\text{NH}_3]$  needed  
436 for nucleation on positive ions to occur (see Section 3) show the usefulness of the first step data  
437 and approximation.

438 As seen from Fig. 4, bonding of  $\text{H}_2\text{SO}_4$  to small negatively charged clusters ( $s < 3$ ) is much  
439 stronger than that to neutrals and positive ions. As a result, at  $s < 3$  the formation of negatively  
440 charged clusters is barrierless ( $\overline{\Delta G_{s-1,s}} < 0$ ). These small clusters cannot be considered as nucleated

441 particles because  $\overline{\Delta G}_{s-1,s}$  (Fig. 4a) first increases and then decreases with growing  $s$ , reaching the  
442 maximum barrier values at  $s = \sim 3 - 6$ .  $\overline{\Delta G}_{s-1,s}$  can become positive for larger clusters due to the  
443 charge effect decreasing quickly as the clusters are growing. ~~The negative  $\overline{\Delta G}_{s-1,s}$  for small~~  
444 ~~clusters is not able to cancel the positive  $\overline{\Delta G}_{s-1,s}$  for larger clusters and thus, to show properly the~~  
445 ~~overall nucleation barrier,  $\overline{\Delta G}_{s-1,s}$  for small clusters are set to zero when they are negative in the~~  
446 ~~cumulative Gibbs free energy calculation.~~ The effect of  $\text{NH}_3$  on negative ions becomes important  
447 at  $s \geq \sim 4$ , when bonding between the clusters and  $\text{NH}_3$  becomes strong enough to contaminate a  
448 large fraction of binary clusters with ammonia (Fig. 3). In contrast, the impact of  $\text{NH}_3$  on neutral  
449 dimers and positively charged monomers of  $\text{H}_2\text{SO}_4$ , as well as on  $\overline{\Delta G}_{s-1,s}$  for both positively  
450 charged and neutral clusters, monotonically decreases for all  $s$ , including  $s \leq 5$ .

451  $\overline{\Delta G}_{s-1,s}$  for charged and neutral clusters converge into the bulk values at  $s = \sim 10$ , when impact  
452 of the chemical identity of the core ion on the cluster composition becomes diffuse (Schobesberger  
453 et al., 2015) and when the contribution of the electrostatic effect to  $\overline{\Delta G}_{s-1,s}$  becomes less than  $\sim$   
454  $0.5 \text{ kcal mol}^{-1}$ . The comparison of cumulative (total)  $\overline{\Delta G}_s$  (Fig. 4b) indicates the lowest nucleation  
455 barrier for the case of negative ions, followed by positive ions and neutrals. The barrierless  
456 formation of clusters with  $s$  ranging from 1 to 3 substantially reduces the nucleation barrier for  
457 negatively charged ions and facilitates their nucleation. The presence of 0.3 ppb of  $\text{NH}_3$  lowers the  
458 nucleation barrier for negative, positive and neutral clusters from  $\sim 17, 24$  and  $38 \text{ kcal mol}^{-1}$  to 2,  
459 7 and  $16 \text{ kcal mol}^{-1}$ , respectively. A relatively low nucleation barrier for charged ternary clusters  
460 is explained by the simultaneous effect of ionization and  $\text{NH}_3$  which also reduces the size of the  
461 critical cluster ( $s^*$ ).

462 It is important to note that the size of the critical cluster, commonly used to “measure” the  
463 activity of nucleation agents in the classical nucleation theory (Coffman and Hegg, 1995;  
464 Korhonen et al., 1999; Vehkamäki et al., 2002; Napari et al., 2002; Hamill et al., 1982) is no longer  
465 a valid indicator, when charged molecular clusters and small nanoparticles are considered. As seen  
466 from Fig. 4, positively charged ternary critical clusters ( $s^* = 3-4$ ) are smaller than the corresponding  
467 negatively charged ones ( $s^* = 4-5$ ); however, the nucleation barrier for ternary positive clusters

468 under the condition specified in the figure caption is more than three times higher than that for  
469 ternary negatives ones.

470

#### 471 2.4.3 Size- and composition- dependent H<sub>2</sub>SO<sub>4</sub> evaporation rates

472 As we mentioned earlier, H<sub>2</sub>SO<sub>4</sub> is the key atmospheric nucleation precursor driving the  
473 formation and growth of clusters in the ternary H<sub>2</sub>SO<sub>4</sub>-H<sub>2</sub>O-NH<sub>3</sub> system while ions, H<sub>2</sub>O, and  
474 NH<sub>3</sub> act to stabilize the H<sub>2</sub>SO<sub>4</sub> clusters. The clustering thermodynamic data derived from QC  
475 calculations and measurements (Section 2.3) are used to constrain size- and composition-  
476 dependent Gibbs free energy changes and evaporation rates of H<sub>2</sub>SO<sub>4</sub> which are critically  
477 important. Average or effective rates of H<sub>2</sub>SO<sub>4</sub> molecule evaporation from positively charged,  
478 negatively charged, and neutral clusters containing  $s$  H<sub>2</sub>SO<sub>4</sub> molecules ( $\bar{\gamma}_s^{+,-,0}$ ) are calculated from

479  $\overline{\Delta G}_{s-1,s}$  as:

$$480 \quad \bar{\gamma}_s^{+,-,0} = \beta_{s-1}^{+,-,0} N^0 \exp\left(\frac{\overline{\Delta G}_{s-1,s}}{RT}\right) \quad (12)$$

481 where  $N^0$  is as defined in Eq. (7). The present model assumes only a single H<sub>2</sub>SO<sub>4</sub> molecule  
482 evaporates, i.e. no water ligands, for instance, are attached to it. This is likely the dominant  
483 evaporation pathway as hydrated H<sub>2</sub>SO<sub>4</sub> molecules are generally more stable.

484 Figure 5 gives the mean evaporation rate ( $\bar{\gamma}$ ) of an H<sub>2</sub>SO<sub>4</sub> molecule from these clusters under  
485 the conditions corresponding to Fig. 4. The shapes of  $\bar{\gamma}$  curves are similar to those of  $\overline{\Delta G}_{s-1,s}$  (Fig.

486 4a) as  $\bar{\gamma}$  values are largely controlled by  $\overline{\Delta G}_{s-1,s}$  (Eq. 12). The presence of ammonia, as expected,

487 significantly reduces the vapor pressure of H<sub>2</sub>SO<sub>4</sub> over bulk aerosol (Marti et al., 1997), and,  
488 hence, the H<sub>2</sub>SO<sub>4</sub> evaporation rate. The evaporation rates of both neutral and positive clusters  
489 decrease as  $s$  increases, and the positive clusters are uniformly more stable than corresponding  
490 neutral clusters.  $\bar{\gamma}$  for negative ions first increases and then decreases as  $s$  increases, peaking  
491 around  $s = \sim 3 - 6$ . The presence of NH<sub>3</sub> reduces the evaporation rates of larger clusters by more  
492 than two orders of magnitude and the effect decreases for smaller clusters, as the binding of NH<sub>3</sub>  
493 to small neutral and charged clusters are weaker compared to that for larger clusters (Fig. 4). [NH<sub>3</sub>]  
494 influences the average NH<sub>3</sub>:H<sub>2</sub>SO<sub>4</sub> ratio (Fig. 3) and the evaporation rates of these small clusters.  
495 The nucleation rates, limited by formation of small clusters ( $s < \sim 5$ ), depend strongly on the  
496 stability or evaporation rate of these small clusters. While the binding of NH<sub>3</sub> to small neutral and  
497 charged clusters is weaker compared to that to larger clusters, small clusters containing NH<sub>3</sub> are  
498 much more stable than those without (Fig. 4) and thus ammonia is important for nucleation.

499

### 500 3. TIMN rates and comparisons with CLOUD measurements

501 The evolution of cluster/particle size distributions can be obtained by solving the dynamic  
502 equations 1-6. Since the concentrations of clusters of all sizes are predicted, the nucleation rates in  
503 the kinetic model can be calculated for any cluster size larger than the critical size of neutral  
504 clusters ( $i > i^*$ ) (Yu, 2006b),

$$505 \quad J_i = J_i^+ + J_i^- + J_i^0 = \beta_{i,1}^+ N_1^0 N_i^+ - \gamma_i^+ N_{i+1}^+ + \beta_{i,1}^- N_1^0 N_i^- - \gamma_i^- N_{i+1}^- + \beta_{i,1}^0 N_1^0 N_i^0 - \gamma_i^0 N_{i+1}^0 \quad (13)$$

506 where  $J_i^+$ ,  $J_i^-$ , and  $J_i^0$  are nucleation rates associated with positive, negative, and neutral clusters  
507 containing  $i$  H<sub>2</sub>SO<sub>4</sub> molecules. As a result of scavenging by pre-existing particles or wall loss, the  
508 steady state  $J_i$  decreases as  $i$  increases. To compare with CLOUD measurements, we calculate  
509 nucleation at cluster mobility diameter of 1.7 nm ( $J_{1.7}$ ).

510 Many practical applications require information on the steady state nucleation rates. For each  
511 nucleation case presented in this paper, constant values of [H<sub>2</sub>SO<sub>4</sub>] (i.e.,  $N_1^0$ ), [NH<sub>3</sub>], T, RH, Q,  
512 and  $L_i^{+, -, 0}$  are assumed. The pre-existing particles with fixed surface area or wall loss serve as a  
513 sink for all clusters. Under a given condition, cluster distribution and nucleation rate reach steady  
514 state after a certain amount of time. We calculate size-dependent coefficients for a given case, and  
515 then solve equations (1-6) to obtain the steady state cluster distribution and nucleation rate, with  
516 the approach described in Yu (2006b).

517 Figure 6 shows a comparison of the model TIMN rates  $J_{1.7}$  with CLOUD measurements, as a  
518 function of [NH<sub>3</sub>] under two ionization rates. It should be noted that Dunne et al. (2016) developed  
519 a simple empirical parameterization (denoted thereafter as “CLOUDpara”) of binary, ternary and  
520 ion-induced nucleation rates in CLOUD measurements as a function of [NH<sub>3</sub>], [H<sub>2</sub>SO<sub>4</sub>], T, and  
521 negative ion concentration. The predictions of CLOUDpara (Dunne et al., 2016) and ACDC based  
522 on nucleation thermochemistry obtained using RI-CC2//B3LYP method (McGrath et al., 2012;  
523 Kurten et al., 2016) are also presented in Fig. 6 for comparisons.

524 Like the CLOUD measurements, the TIMN predictions reveal a complex dependence of  $J_{1.7}$   
525 on [NH<sub>3</sub>], and an analysis of the TIMN results shows this behavior can be explained by the  
526 differing responses of negative, positive and neutral clusters to the presence of ammonia (Fig. 4).  
527 Under the conditions specified in Fig. 6, nucleation is dominated by negative ions for [NH<sub>3</sub>]  $< \sim 0.5$   
528 ppb, by both negative and positive ions for [NH<sub>3</sub>] from  $\sim 0.5$  ppb to  $\sim 10$  ppb (with background  
529 ionization), or  $\sim 20$  ppb (with pion-enhanced ionization), and by neutrals at higher [NH<sub>3</sub>].  
530 According to TIMN, [NH<sub>3</sub>] of at least 0.6–1 ppb are needed before positive ions contribute  
531 significantly to nucleation rates – in good agreement with the threshold found in the CLOUD

532 experiments (Kirkby et al., 2011; Schobesberger et al., 2015). TIMN simulations also extend  
533 CLOUD data at  $[\text{NH}_3]$  of  $\sim 1$  ppb to include a “zero-sensitivity zone” in the region of 1-10 ppb,  
534 followed by a region of strong sensitivity of  $J_{1.7}$  to  $[\text{NH}_3]$  commencing at  $[\text{NH}_3] > \sim 10$ -20 ppb. The  
535 latter zone may have important implications for NPF in heavily polluted regions, including much  
536 of India and China, where  $[\text{NH}_3]$  may exceed 10-20 ppb (Behera and Sharma, 2010; Meng et al.,  
537 2017). It is noteworthy in Fig. 6 that the dependence of  $J_{1.7}$  on  $[\text{NH}_3]$  and  $Q$  predicted by the ACDC  
538 model (McGrath et al., 2012) and the CLOUD data parameterization (Dunne et al., 2016) deviate  
539 substantially from the experimental data as well as the TIMN simulations. The CLOUDpara does  
540 not consider impacts of positive ions and such key controlling parameters as RH and surface area  
541 of pre-existing particles. Dunne et al. (2016) reported that CLOUDpara is also very sensitive to  
542 the approach to parameterize  $T$  dependence, showing that the contribution of ternary ion-induced  
543 nucleation to NPF below 15 km altitude has grown from 9.6% to 37.5%, after the initial empirical  
544 temperature function was replaced with a simpler one.

545 Figure 7 presents a more detailed comparison of TIMN simulations with CLOUD  
546 measurements of  $J_{1.7}$  as a function of  $[\text{H}_2\text{SO}_4]$ ,  $T$ , and RH. The TIMN model reproduces both the  
547 absolute values of  $J_{1.7}$  and its dependencies on  $[\text{H}_2\text{SO}_4]$ ,  $T$ , and RH, in a wide range of  
548 temperatures ( $T=208 - 292$  K) and  $[\text{H}_2\text{SO}_4]$  ( $5 \times 10^5 - 5 \times 10^8 \text{ cm}^{-3}$ ). As expected, nucleation rates  
549 are very sensitive to  $[\text{H}_2\text{SO}_4]$  and  $T$ . For example,  $J_{1.7}$  increases by three to five orders of magnitude  
550 with an increase in  $[\text{H}_2\text{SO}_4]$  of a factor of 10, and by roughly one order of magnitude for a  
551 temperature decrease of 10 degree, except in cases where the nucleation rate is limited by  $Q$  (for  
552 example,  $[\text{H}_2\text{SO}_4] = \sim 10^8 - 10^9 \text{ cm}^{-3}$  at  $T=278$  K and 292 K, shown in Fig. 7a). The key difference  
553 between CLOUDpara and TIMN predictions is that  $\text{dln}J_{1.7}/\text{dln}[\text{H}_2\text{SO}_4]$  ratio predicted by  
554 CLOUDpara is nearly constant while TIMN shows that this ratio depends on both  $[\text{H}_2\text{SO}_4]$  and  $T$ .  
555 The CLOUD measurements taken at  $T=278$  K clearly show (in agreement with the TIMN) that  
556  $\text{dln}J_{1.7}/\text{dln}[\text{H}_2\text{SO}_4]$  is not constant. CLOUDpara overestimates  $J_{1.7}$  compared to both  
557 measurements and TIMN simulations, except for the case, when  $T=278$  K and  $[\text{H}_2\text{SO}_4]$  ranges  
558 from  $\sim 7 \times 10^6$  to  $5 \times 10^7 \text{ cm}^{-3}$ , with deviation of CLOUDpara from experimental data and TIMN  
559 growing with the lower temperature.

560 Both CLOUD measurements and TIMN simulations (Fig. 7b) show an important influence of  
561 RH on nucleation rates ~~(which is neglected in both the CLOUDpara and ACDC models)~~. In  
562 particular, CLOUD measurements indicate 1-5 order of magnitude rise in  $J_{1.7}$  after RH increases  
563 from 10% to 70-80% and a stronger effect of RH on nucleation rates at higher temperatures under  
564 the conditions shown in Fig. 7b. The RH dependence of  $J_{1.7}$  predicted by the TIMN model is  
565 consistent with measurements, being slightly weaker than the measured at high RH.

566 Figure 8 compares TIMN model predictions with all 377 data points of CLOUD measurements  
567 reported in data Table S1 of Dunne et al. (2016). The vertical error bars show the range of  $J_{\text{model}}$

568 associated with the uncertainty in the  $[\text{H}_2\text{SO}_4]$  measured (-50%, +100%). The effect of uncertainty  
569 in measured  $[\text{NH}_3]$  (-50%, +100%) is not included. At the presence of ionization (Fig. 8a),  $J_{\text{model}}$   
570 agrees with CLOUD measurements within the uncertainties under mainly all conditions, although  
571  $J_{\text{model}}$  tends to be slightly lower than  $J_{\text{obs}}$  when  $T=292 - 300$  K and  $J_{\text{obs}}$  is relatively small ( $< \sim 1 \text{ cm}^{-3} \text{ s}^{-1}$ ).  
572 For the neutral nucleation (Fig. 8b), the model agrees well with observations at low  $T$  ( $T=205$   
573  $- 223$  K) but deviates from observations as  $T$  increases. The under-prediction of the model for  
574 neutral nucleation at  $T=278 - 300$  K cannot be explained by the uncertainties in measured  $[\text{H}_2\text{SO}_4]$   
575 and  $[\text{NH}_3]$ . Apparently for neutral nucleation the model predicts much stronger temperature  
576 dependence than the CLOUD measurements. The possible reasons for the difference include the  
577 uncertainties in both the model (especially the thermodynamics data and approximation) and  
578 measurements. It should be noted that, under the conditions of high  $T$  and absence of ions, the role  
579 of cluster evaporation (i.e. thermodynamics) becomes more important (i.e. higher evaporation  
580 and/or generally less tightly bound clusters) and the effect of the possible biases of the used  
581 thermochemistry can be more clearly revealed. The contamination (by amines) in the CLOUD  
582 measurements (Kirkby et al., 2011) can be another possible reason. The level of contamination in  
583 the cloud chamber appears to increase with temperature (Kurten et al., 2016), which may explain  
584 the good agreement at low  $T$  and increased deviation at higher  $T$ . Further research is needed to  
585 identify the source of the difference for neutral ternary nucleation at high  $T$ .

586

#### 587 4. Summary

588 A comprehensive kinetically-based  $\text{H}_2\text{SO}_4\text{-H}_2\text{O-NH}_3$  ternary ion-mediated nucleation (TIMN)  
589 model, constrained with thermodynamic data from quantum-chemical calculations and laboratory  
590 measurements, has been developed and used to shed a new light on physico-chemical processes  
591 underlying the effect of ammonia on NPF. We show that the stabilizing effect of  $\text{NH}_3$  grows with  
592 the cluster size, and that the reduced effect of ammonia on smaller clusters is caused by weaker  
593 bonding that in turn yields lower average  $\text{NH}_3$  to  $\text{H}_2\text{SO}_4$  ratios.  $\text{NH}_3$  was found to impact nucleation  
594 barriers for neutral, positively charged, and negatively charged clusters differently due to the large  
595 difference in the binding energies of  $\text{NH}_3$ ,  $\text{H}_2\text{O}$ , and  $\text{H}_2\text{SO}_4$  to small clusters of different charging  
596 states. The lowest and highest nucleation barriers are observed in the case of negative ions and  
597 neutrals, respectively. Therefore, nucleation of negative ions is favorable, followed by nucleation  
598 of positive ions and neutrals. Different responses of negative, positive and neutral clusters to  
599 ammonia result in a complex dependence of ternary nucleation rates on  $[\text{NH}_3]$ . The TIMN model  
600 reproduces both the absolute values of nucleation rates and their dependencies on the key  
601 controlling parameters and agrees with the CLOUD measurements for all the cases at the presence  
602 of ionization. For the neutral ternary nucleation, the model agrees well with observations at low  
603 temperature but deviates from observations as temperature increases.



604 The TIMN model developed in the present study may subject to uncertainties associated with  
605 the uncertainties in thermodynamic data and interpolation approximation for pre-nucleation  
606 clusters. Further measurements and quantum calculations, especially for relatively larger clusters,  
607 are needed to reduce the uncertainties. While the TIMN model predicts nucleation rates in a good  
608 overall agreement with the CLOUD measurements, its ability to explain the NPF events observed  
609 in the real atmosphere is yet to be quantified and will be investigated in further studies.

610

## 611 **Appendix**

### 612 A1. Quantum-chemical studies of neutral and charged binary and ternary clusters

613 Thermochemical data for small neutral and charged binary  $\text{H}_2\text{SO}_4\text{-H}_2\text{O}$  and ternary  $\text{H}_2\text{SO}_4\text{-}$   
614  $\text{H}_2\text{O-NH}_3$  clusters has been reported in a number of earlier publications (Bandy and Ianni, 1998;  
615 Ianni and Bandy, 1999; Torpo et al., 2007; Nadykto et al., 2008; Herb et al., 2011, 2013; Temelso  
616 et al., 2012a, b; DePalma et al., 2012; Ortega et al., 2012; Chon et al., 2014; Husar et al., 2014;  
617 Henschel et al., 2014, 2016; Kurten et al., 2015). The PW91PW91/6-311++G(3df,3pd) method,  
618 which is a combination of the Perdue-Wang PW91PW91 density functional with the largest Pople  
619 6-311++G(3df,3pd) basis set, has thoroughly been validated and agrees well with existing  
620 experimental data. In earlier studies, this method has been applied to a large variety of  
621 atmospherically-relevant clusters (Nadykto et al. 2006, 2007a, b, 2008, 2014, 2015; Torpo et al.  
622 2007; Zhang et al., 2009; Elm et al. 2012; Leverentz et al. 2013; Xu and Zhang, 2012; Xu and  
623 Zhang, 2013; Elm et al., 2013; Zhu et al. 2014; Bork et al. 2014; Elm and Mikkelsen, 2014; Peng  
624 et al. 2015; Miao et al 2015; Chen et al., 2015; Ma et al., 2016) and has been shown to be well  
625 suited to study the  $\text{H}_2\text{SO}_4\text{-H}_2\text{O}$  and  $\text{H}_2\text{SO}_4\text{-H}_2\text{O-NH}_3$  clusters, as evidenced by a very good  
626 agreement of the computed values with measured cluster geometries, vibrational fundamentals,  
627 dipole properties and formation Gibbs free energies (Nadykto et al., 2007a, b, 2008, 2014, 2015;  
628 Herb et al., 2013; Elm et al., 2012, 2013; Leverentz et al., 2013; Bork et al., 2014) and with high  
629 level ab initio results (Temelso et al., 2012a, b; Husar et al., 2012; Bustos et al., 2014).

630 We have extended the earlier QC studies of binary and ternary clusters to larger sizes. The  
631 computations have been carried out using Gaussian 09 suite of programs (Frisch et al., 2009). In  
632 order to ensure the quality of the conformational search we have carried out a thorough sampling  
633 of conformers. We have used both basin hopping algorithm, as implemented in Biovia Materials  
634 Studio 8.0, and locally developed sampling code. The sampling code is based on the following  
635 principle: mesh, with molecule to be added to the cluster placed in the mesh nodes, is created  
636 around the cluster, and blind search algorithm is used to generate the guess geometries. The mesh  
637 density and orientation of molecules are variable, as well as the minimum distance between  
638 molecules and cluster. Typically, for each cluster of a given chemical composition a thousand to  
639 several thousands of isomers have been sampled. We used a three-step optimization procedure,

640 which includes (i) pre-optimization of initial/guess geometries by semi-empirical PM6 method,  
641 separation of the most stable isomers located within 15 kcal mol<sup>-1</sup> of the intermediate global  
642 minimum and duplicate removal, followed by (ii) optimization of the selected isomers meeting the  
643 aforementioned stability criterion by PW91PW91/CBSB7 method and (iii) the final optimization  
644 of the most stable at PW91PW91/CBSB7 level isomers within 5 kcal mol<sup>-1</sup> of the current global  
645 minimum using PW91PW91/6-311++G(3df,3pd) method. Typically, only ~4-30% of initially  
646 sampled isomers reach the second (PW91PW91/CBSB7) level, where ~10-40% of isomers  
647 optimized with PW91PW91/CBSB7 are selected for the final run. Typically, the number of  
648 equilibrium isomers of hydrated clusters is larger than that of unhydrated ones of similar chemical  
649 composition. Table A1 shows the numbers of isomers converged at the final PW91PW91/6-  
650 311++G(3df,3pd) optimization step for selected clusters and HSG values of the most stable  
651 isomers used in the present study. The number of isomers optimized at the PW91PW91/6-  
652 311++G(3df,3pd) level of theory varies from case to case, typically being in the range of ~10-200.

653 The computed stepwise enthalpy, entropy, and Gibbs free energies of cluster formation have  
654 been thoroughly evaluated and used to calculate the evaporation rates of H<sub>2</sub>SO<sub>4</sub> from neutral,  
655 positive and negative charged clusters.

656

#### 657 A1.1 Positively charged clusters

658 Table A2 presents the computed stepwise Gibbs free energy changes under standard conditions  
659 ( $\Delta G^{\circ}$ ) for positive binary and ternary clusters, along with the corresponding experimental data or  
660 semi-experimental estimates. Figure 2 in the main text shows  $\Delta G$  associated with the addition of  
661 water ( $\Delta G_{+W}^{\circ}$ ), ammonia ( $\Delta G_{+A}^{\circ}$ ), and sulfuric acid ( $\Delta G_{+S}^{\circ}$ ) to binary and ternary clusters as a  
662 function of the cluster hydration number  $w$ . Both the absolute values and trends in  $\Delta G_{+W}^{\circ}$  derived  
663 from calculations are in agreement with the laboratory measurements within the uncertainty range  
664 of ~1-2 kcal mol<sup>-1</sup> for both QC calculations and measurements. This confirms the efficiency and  
665 precision of QC methods in calculating thermodynamic data needed for the development of  
666 nucleation models. Nevertheless, it should be noted that the uncertainties in computed free energies  
667 of 1-2 kcal mol<sup>-1</sup> may lead to large uncertainty in predicted particle formation rates. By increasing  
668 or decreasing all Gibbs free energies by 1 kcal mol<sup>-1</sup>, Kürten et al. (2016) showed that, depending  
669 on the conditions, the modeled particle formation rate can change from less than an order of  
670 magnitude to several orders of magnitude. Uncertainties estimated by Kürten et al. (2016)  
671 represent the upper limit because computed free energies may be overestimated for some clusters  
672 and underpredicted for others that leads to partial or, in some case, full error cancellation.

673

#### 674 A1.2 Neutral clusters

675 Table A3 presents the computed stepwise Gibbs free energy changes for the formation of  
676 ternary  $S_sA_aW_w$  clusters under standard conditions. The corresponding binary electrically neutral  
677 clusters can be found in previous publications (e.g., Nadykto et al., 2008; Herb et al., 2011). The  
678 thermodynamic properties of the  $S_1A_1$  have been reported in a number of computational studies  
679 (e.g., Herb et al., 2011; Kurten et al., 2007; Nadykto and Yu, 2007). However, most of these  
680 studies, except for Nadykto and Yu (2007) and Henschel et al. (2014; 2016), did not consider the  
681 impact of  $H_2O$  on cluster thermodynamics. We have extended the earlier studies of Nadykto and  
682 Yu (2007) and Herb et al. (2011) to larger clusters up to  $S_4A_5$  (no hydration) and up to  $S_2A_2$   
683 (hydration included). The free energy of binding of  $NH_3$  to  $H_2SO_4$  (or  $H_2SO_4$  to  $NH_3$ ) obtained  
684 using our method is  $-7.77 \text{ kcal mol}^{-1}$  that is slightly more negative than values reported by other  
685 groups ( $-6.6$   $-7.61 \text{ kcal mol}^{-1}$ ) and within less than  $0.5 \text{ kcal mol}^{-1}$  of the experimental value of  $-$   
686  $8.2 \text{ kcal mol}^{-1}$  derived from CLOUD measurements (Kurten et al., 2015).

687 As it may be seen from Table A3, the  $NH_3$  binding to  $S_{1-2}W_w$  weakens as  $w$  increases. The  
688 average  $\Delta G_{+W}^0$  for  $S_1W_w$  formation derived from a combination of laboratory measurements and  
689 quantum chemical studies are  $-3.02$ ,  $-2.37$ , and  $-1.40 \text{ kcal mol}^{-1}$  for the first, second, and third  
690 hydration, respectively (Yu, 2007). This indicates that a large fraction of  $H_2SO_4$  monomers in the  
691 Earth's atmosphere is likely hydrated. Therefore, the decreasing  $NH_3$  binding strength to hydrated  
692  $H_2SO_4$  monomers implies that RH (and T) will affect the relative abundance of  $H_2SO_4$  monomers  
693 containing  $NH_3$ . Currently, no experimental data or observations are available to evaluate the  
694 impact of hydration (or RH) on  $\Delta G_{+A}^0$ . Table A3 shows that the presence of  $NH_3$  in  $H_2SO_4$  clusters  
695 suppress hydration and that  $\Delta G_{+W}^0$  for  $S_2A_2$  falls below  $-2.0 \text{ kcal mol}^{-1}$ . This is consistent with  
696 earlier studies by our group (Herb et al., 2011) and others (Henschel et al., 2014, 2016) showing  
697 that large  $S_nA_n$  clusters ( $n > 2$ ) are not hydrated under typical atmospheric conditions. In the present  
698 study, the hydration of neutral  $S_nA_n$  clusters at  $n > 2$  is neglected, due to the lack of thermodynamic  
699 data.

700 The number of  $NH_3$  molecules in the cluster (or  $H_2SO_4$  to  $NH_3$  ratio) significantly affects  $\Delta G_{+S}^0$   
701 and  $\Delta G_{+A}^0$  values. For example,  $\Delta G_{+S}^0$  for  $S_3A_a$  clusters increases from  $-7.08 \text{ kcal mol}^{-1}$  to  $-16.92$   
702  $\text{kcal mol}^{-1}$  and  $\Delta G_{+A}^0$  decreases from  $-16.14 \text{ kcal mol}^{-1}$  to  $-8.93 \text{ kcal mol}^{-1}$  as  $a$  is growing from 1  
703 to 3. For  $S_4A_a$  clusters,  $\Delta G_{+S}^0$  is increasing from  $-7.48 \text{ kcal mol}^{-1}$  to  $-16.26 \text{ kcal mol}^{-1}$  and  $\Delta G_{+A}^0$   
704 decreases from  $-17.16 \text{ kcal mol}^{-1}$  to  $-11.34 \text{ kcal mol}^{-1}$  as  $a$  increases from 2 to 4.  $\Delta G_{+A}^0$  for  $S_4A_1$   
705 cluster is by  $1.38 \text{ kcal mol}^{-1}$  less negative than that for  $S_4A_2$ .  $\Delta G_{+S}^0$  for the  $S_4A_1$  cluster is also quite  
706 low ( $-4.16 \text{ kcal mol}^{-1}$ ) that might indicate the possible existence of a more stable  $S_4A_1$  isomer,  
707 which is yet to be identified. In the presence of  $NH_3$ , the uncertainty in the thermochemistry data  
708 for  $S_4A_1$  will not significantly affect ternary nucleation rates because most of  $S_4$ -clusters contain  
709 3 or 4  $NH_3$  molecules.

710 For the  $S_sA_a$  clusters with  $s=a$ ,  $\Delta G_{+A}^0$  increases as cluster is growing while  $\Delta G_{+S}^0$  first increases  
711 significantly as  $S_1A_1$  is converting into  $S_2A_2$  and then levels off as  $S_2A_2$  is converting into  $S_4A_4$ .  
712 We also observe a significant drop in  $\Delta G_{+A}^0$  in the case when  $NH_3/H_2SO_4$  ratio exceeds 1. This  
713 finding is consistent with the ACDC model calculation showing that growth of neutral  $S_sA_a$   
714 clusters follows the  $s=a$  pathway (Schobesberger et al., 2015).

715

### 716 A1.3 Negative ionic clusters

717 Table A4 shows  $\Delta G_{+W}$ ,  $\Delta G_{+A}$ , and  $\Delta G_{+S}$  needed to form negatively charged clusters under  
718 standard conditions, along with available semi-experimental values (Froyd and Lovejoy, 2003).  
719  $H_2O$  binding to negatively charged  $S^-S_s$  clusters significantly strengthens with increasing  $s$ , from  
720  $\Delta G_{+W}^0 = -0.61$  to  $-1.83$  kcal mol<sup>-1</sup> at  $s=1-2$  to  $\Delta G_{+W}^0 = -3.5$  kcal mol<sup>-1</sup> at  $w=1$  and  $-2.25$  kcal mol<sup>-1</sup> at  
721  $w=4$  at  $s=4$ .  $\Delta G_{+W}^0$  values at  $s=3$  and 4 are slightly more negative (by  $\sim 0.1 - 0.9$  kcal mol<sup>-1</sup>) than  
722 those reported by Froyd and Lovejoy (2003). Just like  $H_2O$  binding,  $NH_3$  binding to  $S^-S_s$  at  $s<3$  is  
723 very weak, with  $\Delta G_{+A}^0$  ranging from  $+2.81$  kcal mol<sup>-1</sup> at  $s=0$  to  $-4.85$  kcal mol<sup>-1</sup> at  $s=2$ . However,  
724 it significantly increases as  $s$  is growing. In particular, at  $s \geq 3$   $\Delta G_{+A}^0$  is ranging from  $-11.89$  kcal  
725 mol<sup>-1</sup> for  $S^-S_3A_1$  to  $-15.37$  kcal mol<sup>-1</sup> for  $S^-S_4A_1$ .  $NH_3$  clearly cannot get into small negative ions.  
726 However, it can easily attach to larger negative ions with  $s \geq 3$  that is consistent with CLOUD  
727 measurements (Schobesberger et al., 2015). Since hydration weakens  $NH_3$  binding in  $S^-S_3A_1W_w$   
728 and  $S^-S_4A_1W_w$  clusters, its impacts on the cluster formation and nucleation rates may potentially  
729 be important.

730 In contrast to  $H_2O$  and  $NH_3$ , binding of  $H_2SO_4$  to small negative ions ( $s<3$ ) is very strong.  
731 These ions are very stable even when they contain no  $NH_3$  or  $H_2O$  molecules. High electron  
732 affinity of  $H_2SO_4$  molecules results in the high stability of  $S^-S_s$  at  $s=1-2$ . However, the charge  
733 effect reduces as  $s$  is growing. In particular,  $\Delta G_{+S}^0$  of  $S^-S_s$  drops from  $-32.74$  kcal mol<sup>-1</sup> at  $s=1$  to  
734  $-10.58$  kcal mol<sup>-1</sup> and  $-8.28$  kcal mol<sup>-1</sup> at  $s=3$  and 4, respectively. At the same time,  $\Delta G_{+A}^0$  increases  
735 from  $0.08$  kcal mol<sup>-1</sup> ( $s=1$ ) to  $-11.89$  kcal mol<sup>-1</sup> ( $s=3$ ) and  $-15.37$  kcal mol<sup>-1</sup> ( $s=4$ ). The hydration  
736 of  $S^-S_s$  at  $s=3, 4$  enhances the strength of  $H_2SO_4$  binding, especially at  $s=4$ .  $\Delta G_{+S}^0$  values for  $S^-S_3-$   
737  $4W_w$  are consistently  $\sim 1.5 - 3$  kcal mol<sup>-1</sup> less negative than the corresponding semi-experimental  
738 estimates (Table A4). The possible reasons behind the observed systematic difference are yet to  
739 be identified and include the use of low-level *ab initio* HF method to compute reaction enthalpies  
740 and uncertainties in experimental enthalpies in studies by Froyd and Lovejoy (2003).

741  $NH_3$  binding to  $S^-S_3$  significantly enhances the stability of  $H_2SO_4$  in the cluster by  $\sim 7$  kcal mol<sup>-1</sup>  
742 compared to  $\Delta G_{+S}^0$  for the corresponding binary counterpart. The binding of the second  $NH_3$  to  
743  $S^-S_3A$  to form  $S^-S_3A_2$  is much weaker ( $\Delta G_{+A}^0 = -7.27$  kcal mol<sup>-1</sup>) than that of the first  $NH_3$  molecule  
744 ( $\Delta G_{+A}^0 = -11.89$  kcal mol<sup>-1</sup>). This indicates that most of  $S^-S_3A_a$  can only contain one  $NH_3$  molecule,  
745 in a perfect agreement with the laboratory study of Schobesberger et al. (2015). In the case of  $S^-$

746 S<sub>4</sub>, binding of the first ( $\Delta G_{+A}^{\circ} = -15.37 \text{ kcal mol}^{-1}$ ) and second (and  $-12.23 \text{ kcal mol}^{-1}$ ) NH<sub>3</sub>  
747 molecules to the cluster is quite strong, while the attachment of NH<sub>3</sub> leads to substantial  
748 stabilization of H<sub>2</sub>SO<sub>4</sub> in the cluster, as evidenced by  $\Delta G_{+S}^{\circ}$  growing from  $-8.28 \text{ kcal mol}^{-1}$  at  $a=0$   
749 to  $-11.76 \text{ kcal mol}^{-1}$  and  $-16.71 \text{ kcal mol}^{-1}$  at  $a=1$  and  $a=2$ , respectively. The NH<sub>3</sub> binding free  
750 energy to S<sup>-</sup>S<sub>4</sub>A<sub>2</sub> (to form S<sup>-</sup>S<sub>4</sub>A<sub>3</sub>) drops to  $-7.59 \text{ kcal mol}^{-1}$ , indicating, in agreement with the  
751 CLOUD measurements (Schobesberger et al., 2015) that most of S<sup>-</sup>S<sub>4</sub> clusters contain 1 or 2 NH<sub>3</sub>  
752 molecules.

753

754 **Acknowledgments.** The authors thank Richard Turco (Distinguished Professor Emeritus, UCLA)  
755 for comments that helped to improve the manuscript. This study was supported by NSF under  
756 grant 1550816, NASA under grant NNX13AK20G, and NYSERDA under contract 100416. ABN  
757 would like to thank the Russian Science Foundation and the Ministry of Science and Education of  
758 Russia (under grants 1.6198.2017/6.7 and 1.7706.2017/8.9) for support and the Center of  
759 Collective Use of MSTU Stankin for providing resources.

760

761 **Data availability.** All relevant data are available in the article, or from the corresponding authors  
762 upon request.

763

## 764 **References**

765 Almeida, J., et al., Molecular understanding of sulphuric acid–amine particle nucleation in the  
766 atmosphere, *Nature*, 502, 359-363, 2013.

767 Ball, S. M., Hanson, D. R., Eisele, F. L., and McMurry, P. H., Laboratory studies of particle  
768 nucleation: Initial results for H<sub>2</sub>SO<sub>4</sub>, H<sub>2</sub>O, and NH<sub>3</sub> vapors, *J. Geophys. Res.*, 104, 23709-23718,  
769 10.1029/1999JD900411, 1999.

770 Bandy, A.R. and Ianni, J.C., Study of the hydrates of H<sub>2</sub>SO<sub>4</sub> using density functional theory. *The*  
771 *Journal of Physical Chemistry A*, 102(32), pp.6533-6539, 1998.

772 Behera, S. N., and M. Sharma, Investigating the potential role of ammonia in ion chemistry of fine  
773 particulate matter formation for an urban environment, *The Science of the Total Environment*,  
774 408(17), 3569-3575, 2010.

775 Benson, D. R., M. E. Erupe, and S.-H. Lee, Laboratory-measured H<sub>2</sub>SO<sub>4</sub>-H<sub>2</sub>O-NH<sub>3</sub> ternary  
776 homogeneous nucleation rates: Initial observations, *Geophys. Res. Lett.*, 36, L15818,  
777 doi:10.1029/2009GL038728, 2009.

778 Bork, N., Du, L., Reiman, H., Kurtén, T. and Kjaergaard, H.G., Benchmarking ab initio binding  
779 energies of hydrogen-bonded molecular clusters based on FTIR spectroscopy, *Journal of*  
780 *Physical Chemistry A*, 118(28), 5316-5322, 2014.

781 Bustos, D.J., Temelso, B. and Shields, G.C., Hydration of the Sulfuric Acid–Methylamine  
782 Complex and Implications for Aerosol Formation. *The Journal of Physical Chemistry A*,  
783 118(35), pp.7430-7441, 2014.

784 Butler, T., Vermeulen, F., Lehmann, C. M., Likens, G. E., & Puchalski, M.. Increasing ammonia  
785 concentration trends in large regions of the USA derived from the NADP/AMoN network.  
786 *Atmospheric Environment*, 146, 132–140. 2016.

787 Chen, M., M. Titcombe, J. Jiang, C. Kuang, M. L. Fischer, E. Edgerton, F. L. Eisele, J. I. Siepmann,  
788 D. H. Hanson, J. Zhao, and P. H. McMurry, Acid-base chemical reaction model for nucleation  
789 rates in the polluted boundary layer. *Proc. Nat. Acad. Sci.*, 109, 18713–18718, 2012.

790 Chon, N.L., Lee, S.H. and Lin, H., A theoretical study of temperature dependence of cluster  
791 formation from sulfuric acid and ammonia. *Chemical Physics*, 433, pp.60-66, 2014.

792 Coffman, D. J., and Hegg, D. A., A preliminary study of the effect of ammonia on particle  
793 nucleation in the marine boundary layer, *J. Geophys. Res.*, 100, 7147-7160, 1995.

794 Davidson, J. A., Fehsenfeld, F.C., Howard, C.J.: The heats of formation of  $\text{NO}_3^-$  and  $\text{NO}_3^-$   
795 association complexes with  $\text{HNO}_3$  and  $\text{HBr}$ , *Int. J. Chem. Kinet.*, 9, 17, 1977.

796 Dawson M.L., et al., Simplified mechanism for new particle formation from methanesulfonic acid,  
797 amines and water via experiments and ab initio calculations, *Proc Natl Acad Sci USA*  
798 109:18719–18724, 2012.

799 DePalma, J.W., Bzdek, B.R., Doren, D.J. and Johnston, M.V., Structure and energetics of  
800 nanometer size clusters of sulfuric acid with ammonia and dimethylamine, *Journal of Physical*  
801 *Chemistry A*, 116(3), pp.1030-1040, 2012.

802 Doyle, G. J., Self-nucleation in the sulfuric acid-water system, *J. Chem. Phys.*,35, 795–799, 1961.

803 Dunne, E. M., et al., Global particle formation from CERN CLOUD measurements, *Science*,  
804 doi:10.1126/science.aaf2649, 2016.

805 Duplissy J., et al., Effect of ions on sulfuric acid-water binary particle formation: 2. Experimental  
806 data and comparison with QC-normalized classical nucleation theory, *J. Geophys. Res. Atmos.*,  
807 121, 1752–1775, doi:10.1002/2015JD023539, 2016.

808 Elm, J. and Mikkelsen, K.V., Computational approaches for efficiently modelling of small  
809 atmospheric clusters, *Chemical Physics Letters*, 615, 26-29, 2014.

810 Elm, J., Bilde, M. and Mikkelsen, K.V., Assessment of binding energies of atmospherically  
811 relevant clusters, *Physical Chemistry Chemical Physics*, 15(39), 16442-16445, 2013.

812 Elm, J., Bilde, M. and Mikkelsen, K.V., Assessment of density functional theory in predicting  
813 structures and free energies of reaction of atmospheric prenucleation clusters, *Journal of*  
814 *chemical theory and computation*, 8(6), 2071-2077, 2012.

815 Frisch, M. J., Trucks, G. W., Schlegel, H. B., Scuseria, G. E., Robb, M. A., Cheeseman, J. R.,  
816 Scalmani, G., Barone, V., Mennucci, B., et al., Gaussian 09, Gaussian, Inc., Wallingford CT,  
817 2009.

818 Froyd K. D., and Lovejoy E. R., Bond energies and structures of ammonia-sulfuric acid positive  
819 cluster ions, *J. Phys. Chem. A*, 116(24), 5886–5899, doi:10.1021/jp209908f, 2012.

820 Froyd, K. D., and Lovejoy, E. R., Experimental thermodynamics of cluster ions composed of  
821 H<sub>2</sub>SO<sub>4</sub> and H<sub>2</sub>O. 1. Positive ions, *J. Phys. Chem. A*, 107, 9800–9811, 2003.

822 Froyd, K. D., and Lovejoy, E. R., Experimental thermodynamics of cluster ions composed of  
823 H<sub>2</sub>SO<sub>4</sub> and H<sub>2</sub>O. 2. Measurements and ab initio structures of negative ions, *J. Phys. Chem. A*,  
824 107, 9812–9824, 2003.

825 Froyd, K. D., and Lovejoy, E. R., Experimental thermodynamics of cluster ions composed of  
826 H<sub>2</sub>SO<sub>4</sub> and H<sub>2</sub>O. 1. Positive ions, *J. Phys. Chem. A*, 107, 9800–9811, 2003.

827 Froyd, K. D., Ion induced nucleation in the atmosphere: Studies of NH<sub>3</sub>, H<sub>2</sub>SO<sub>4</sub>, and H<sub>2</sub>O cluster  
828 ions, Ph.D. thesis, Univ. of Colo., Boulder, 2002.

829 Glasoe, W. A., Volz, K., Panta, B., Freshour, N., Bachman, R., Hanson, D. R., McMurry, P. H.,  
830 and Jen, C.. Sulfuric acid nucleation: An experimental study of the effect of seven bases. *Journal*  
831 *of Geophysical Research: Atmospheres*, 120(5), 1933-1950, 2015.

832 Hamill, P., Turco, R. P., Kiang, C. S., Toon, O. B., & Whitten, R. C., An analysis of various  
833 nucleation mechanisms for sulfate particles in the stratosphere. *Journal of Aerosol Science*, 13,  
834 561–585, 1982.

835 Hanson, D. R., and F. Eisele, Diffusion of H<sub>2</sub>SO<sub>4</sub> in humidified nitrogen: Hydrated H<sub>2</sub>SO<sub>4</sub>, *J. Phys.*  
836 *Chem. A*, 104, 1715 – 1719, 2000.

837 Hanson, D. R., and F. L. Eisele, Measurement of prenucleation molecular clusters in the NH<sub>3</sub>,  
838 H<sub>2</sub>SO<sub>4</sub>, H<sub>2</sub>O system, *J. Geophys. Res.*, 107(D12), 4158, doi:10.1029/2001JD001100, 2002.

839 Hanson, DR., Lovejoy, ER, Measurement of the thermodynamics of the hydrated dimer and  
840 trimers, *J. Phys. Chem. A* 110: 9525-9538 DOI: 10.1021/jp062844w, 2006.

841 Henschel, H., J. C. A. Navarro, T. Yli-Juuti, O. Kupiainen-Määttä, T. Olenius, I. K. Ortega, S. L.  
842 Clegg, T. Kurtén, I. Riipinen, and H. Vehkamäki, Hydration of atmospherically relevant  
843 molecular clusters: Computational chemistry and classical thermodynamics, *J. Phys. Chem. A*,  
844 118, 2599–2611, 2014.

845 Henschel, H., T. Kurtén, and H. Vehkamäki, Computational study on the effect of hydration on  
846 new particle formation in the sulfuric acid/ammonia and sulfuric acid/dimethylamine systems,  
847 *J. Phys. Chem. A*, 120, 1886–1896, doi:10.1021/acs.jpca.5b11366, 2016.

848 Herb, J., Y. Xu, F. Yu, and A. B. Nadykto, Large Hydrogen-Bonded Pre-Nucleation ( $\text{HSO}_4^-$   
849  $(\text{H}_2\text{SO}_4)_m(\text{H}_2\text{O})_k$  and  $(\text{HSO}_4^-)(\text{NH}_3)(\text{H}_2\text{SO}_4)_m(\text{H}_2\text{O})_k$  Clusters in the Earth's Atmosphere, *J.*  
850 *Phys. Chem., A*, 117, 133-152, DOI: 10.1021/jp3088435, 2013.

851 Herb., J., A. Nadykto, and F. Yu, Large Ternary Hydrogen-Bonded Pre-Nucleation Clusters in the  
852 Earth's Atmosphere, *Chemical Physics Letters*, 518, 7-14, 10.1016/j.cplett.2011.10.035, 2011.

853 Holland, P. M., and Castleman, A. W., Jr.: Thomson equation revisited in light of ion-clustering  
854 experiments, *J. Phys. Chem.*; 86, 4181-4188, 1982.

855 Hoppel, W.A., and G. M. Frick, Ion-aerosol attachment coefficients and the steady-state charge  
856 distribution on aerosols in a bipolar ion environment, *Aerosol Sci. Tech.*, 1-21, 1986.

857 Husar, D.E., Temelso, B., Ashworth, A.L. and Shields, G.C., Hydration of the bisulfate ion:  
858 atmospheric implications. *The Journal of Physical Chemistry A*, 116(21), pp.5151-5163, 2012.

859 Hyvärinen, A., T. Raatikainen, A. Laaksonen, Y. Viisanen, and H. Lihavainen, Surface tensions  
860 and densities of  $\text{H}_2\text{SO}_4 + \text{NH}_3 + \text{water}$  solutions, *Geophys. Res. Lett.*, 32, L16806,  
861 doi:10.1029/2005GL023268, 2005.

862 Ianni, J.C. and Bandy, A.R., A Density Functional Theory Study of the Hydrates of  $\text{NH}_3\text{-H}_2\text{SO}_4$   
863 and Its Implications for the Formation of New Atmospheric Particles. *The Journal of Physical*  
864 *Chemistry A*, 103(15), pp.2801-2811, 1999.

865 Jacobson, M., Turco, R., Jensen, E. and Toon O.: Modeling coagulation among particles of  
866 different composition and size, *Atmos. Environ.*, 28, 1327-1338, 1994.

867 Jolly, William L., *Modern Inorganic Chemistry (2nd Edn.)*. New York: McGraw-Hill. ISBN 0-07-  
868 112651-1, 1991.

869 Kazil, J., Lovejoy, E. R., Jensen, E. J., and Hanson, D. R.: Is aerosol formation in cirrus clouds  
870 possible?, *Atmos. Chem. Phys.*, 7, 1407-1413, <https://doi.org/10.5194/acp-7-1407-2007>, 2007.

871 Kebarle, P., S. K. Searles, A. Zolla, J. Scarborough, and M. Arshadi, *J. Am. Chem. Soc.*, 89, 6393,  
872 1967.

873 Kim, T. O., T. Ishida, M. Adachi, K. Okuyama, and J. H. Seinfeld, Nanometer-Sized Particle  
874 Formation from  $\text{NH}_3/\text{SO}_2/\text{H}_2\text{O}/\text{Air}$  Mixtures by Ionizing Irradiation, *Aerosol Science and*  
875 *Technology*, 29, 112-125, 1998.

876 Kirkby, J., Curtius, J., Almeida, J., Dunne, E., Duplissy, J., et al., The role of sulfuric acid,  
877 ammonia and galactic cosmic rays in atmospheric aerosol nucleation, *Nature*, 476, 429-433,  
878 2011.

879 Korhonen, P., Kulmala, M., Laaksonen, A., Viisanen, Y., McGraw, R., and Seinfeld, J. H., Ternary  
880 nucleation of  $\text{H}_2\text{SO}_4$ ,  $\text{NH}_3$ , and  $\text{H}_2\text{O}$  in the atmosphere, *J. Geophys. Res.*, 104, 26,349-26,353,  
881 1999.



882 Kurtén, T., Torpo, L., Ding, C.-G., Vehkamäki, H., Sundberg, M. R., Laasonen, K., and Kulmala,  
883 M.: A density functional study on water-sulfuric acid-ammonia clusters and implications for at-  
884 mospheric cluster formation, *J. Geophys. Res.*, 112, D04210, doi:10.1029/2006JD007391,  
885 2007.

886 Kürten, A., et al., Experimental particle formation rates spanning tropospheric sulfuric acid and  
887 ammonia abundances, ion production rates, and temperatures, *J. Geophys. Res. Atmos.*, 121,  
888 12,377–12,400, doi:10.1002/2015JD023908, 2016.

889 Kürten, A., Münch, S., Rondo, L., Bianchi, F., Duplissy, J., Jokinen, T., Junninen, H., Sarnela, N.,  
890 Schobesberger, S., Simon, M. and Sipilä, M., Thermodynamics of the formation of sulfuric acid  
891 dimers in the binary (H<sub>2</sub>SO<sub>4</sub>–H<sub>2</sub>O) and ternary (H<sub>2</sub>SO<sub>4</sub>–H<sub>2</sub>O–NH<sub>3</sub>) system. *Atmospheric*  
892 *Chemistry and Physics*, 15(18), pp.10701-10721, 2015.

893 Laakso, L., Mäkelä, J. M., Pirjola, L., and Kulmala, M., Model studies of ion-induced nucleation  
894 in the atmosphere, *J. Geophys. Res.*, 107, 4427, doi:10.1029/2002JD002140, 2003.

895 Leverentz, H.R., Siepmann, J.I., Truhlar, D.G., Loukonen, V. and Vehkamäki, H., Energetics of  
896 atmospherically implicated clusters made of sulfuric acid, ammonia, and dimethyl amine,  
897 *Journal of Physical Chemistry A*, 117(18), 3819-3825, 2013.

898 Lovejoy, E. R., Curtius, J., and Froyd, K. D., Atmospheric ion-induced nucleation of sulfuric acid  
899 and water, *J. Geophys. Res.*, 109, D08204, doi:10.1029/2003JD004460, 2004.

900 Ma, Y., Chen, J., Jiang, S., Liu, Y.R., Huang, T., Miao, S.K., Wang, C.Y. and Huang, W.,  
901 Characterization of the nucleation precursor (H<sub>2</sub>SO<sub>4</sub>–(CH<sub>3</sub>)<sub>2</sub>NH) complex: intra-cluster  
902 interactions and atmospheric relevance. *RSC Advances*, 6(7), pp.5824-5836, 2016.

903 Marti, J. J., A. Jefferson, X. Ping Cai, C. Richert, P. H. McMurry, and F. Eisele, H<sub>2</sub>SO<sub>4</sub> vapor  
904 pressure of sulfuric acid and ammonium sulfate solutions, *J. Geophys. Res.*, 102(D3), 3725–3736,  
905 1997.

906 McGrath, M. J., Olenius, T., Ortega, I. K., Loukonen, V., Paasonen, P., Kurtén, T., Kulmala, M.,  
907 and Vehkamäki, H.: Atmospheric Cluster Dynamics Code: a flexible method for solution of the  
908 birth-death equations, *Atmos. Chem. Phys.*, 12, 2345-2355, doi:10.5194/acp-12-2345-2012,  
909 2012.

910 Meng, Z., Xu, X., Lin, W., Xie, Y., Song, B., Jia, S., Zhang, R., Peng, W., Wang, Y., Cheng, H.,  
911 Yang, W., and Zhao, H., Role of ambient ammonia in particulate ammonium formation at a rural  
912 site in the North China Plain, *Atmos. Chem. Phys. Discuss.*, [https://doi.org/10.5194/acp-2017-](https://doi.org/10.5194/acp-2017-174)  
913 174, in review, 2017.

914 Meot-Ner (Mautner), M., The Ionic Hydrogen Bond and Ion Solvation. 2. Hydration of Onium  
915 Ions by 1 - 7 H<sub>2</sub>O Molecules. Relations Between Monomolecular, Specific and Bulk Hydration,  
916 *J. Am. Chem. Soc.*, 106, 5, 1265, 1984.

917 Merikanto J., I. Napari, H. Vehkamäki, T. Anttila, M. Kulmala, New parameterization of sulfuric  
918 acid-ammonia-water ternary nucleation rates at tropospheric conditions, *J. Geophys. Res.*, 112,  
919 D15207, doi:10.1029/2006JD007977, 2007.

920 Miao, S.K., Jiang, S., Chen, J., Ma, Y., Zhu, Y.P., Wen, Y., Zhang, M.M. and Huang, W.,  
921 Hydration of a sulfuric acid–oxalic acid complex: acid dissociation and its atmospheric  
922 implication, *RSC Advances*, 5(60), 48638-48646, 2015.

923 Nadykto, A. B., A. Al Natsheh, F. Yu, K.V. Mikkelsen, and J. Herb, *Computational Quantum*  
924 *Chemistry: A New Approach to Atmospheric Nucleation*, *Advances in Quantum Chemistry*, 55,  
925 449-478, 2008.

926 Nadykto, A. B., Al Natsheh, A., Yu, F., Mikkelsen, K. V., and Ruuskanen, J., Quantum nature of  
927 the sign preference in the ion-induced nucleation, *Physical Review Letters*, 96, 125701, 2006.

928 Nadykto, A., and Yu, F., Uptake of neutral polar vapour molecules by charged particles:  
929 Enhancement due to dipole-charge interaction, *J. Geophys. Res.*, 108(D23), 4717,  
930 doi:10.1029/2003JD003664, 2003.

931 Nadykto, A.B. and Yu, F., Strong hydrogen bonding between atmospheric nucleation precursors  
932 and common organics. *Chemical physics letters*, 435(1), pp.14-18, 2007a.

933 Nadykto, A.B., Du, H. and Yu, F., Quantum DFT and DF–DFT study of vibrational spectra of  
934 sulfuric acid, sulfuric acid monohydrate, formic acid and its cyclic dimer. *Vibrational*  
935 *spectroscopy*, 44(2), pp.286-296, 2007b.

936 Nadykto, A. B., F. Yu, and J. Herb, Theoretical analysis of the gas-phase hydration of common  
937 atmospheric pre-nucleation  $(\text{HSO}_4^-)(\text{H}_2\text{O})_n$  and  $(\text{H}_3\text{O}^+)(\text{H}_2\text{SO}_4)(\text{H}_2\text{O})_n$  cluster ions, *Chemical*  
938 *Physics*, 360, 67-73, doi:10.1016/j.chemphys.2009.04.007, 2009.

939 Nadykto, A.B., Herb, J., Yu, F. and Xu, Y., Enhancement in the production of nucleating clusters  
940 due to dimethylamine and large uncertainties in the thermochemistry of amine-enhanced  
941 nucleation. *Chemical Physics Letters*, 609, 42-49, 2014.

942 Nadykto, A.B., Herb, J., Yu, F., Nazarenko, E.S. and Xu, Y., Reply to the ‘Comment on  
943 “Enhancement in the production of nucleating clusters due to dimethylamine and large  
944 uncertainties in the thermochemistry of amine-enhanced nucleation”’ by Kupiainen-Maatta et al.  
945 *Chemical Physics Letters*, 624, 111-118, 2015.

946 Napari, I, Noppel, M, Vehkamäki, H., Kulmala, M., An improved model for ternary nucleation of  
947 sulfuric acid–ammonia–water. *J. Chem. Phys.*, 116: 4221-4227, DOI: 10.1063/1.1450557, 2002.

948 Olenius T., O. Kupiainen-Määttä, I. K. Ortega, T. Kurtén, and H. Vehkamäki, Free energy barrier  
949 in the growth of sulfuric acid–ammonia and sulfuric acid–dimethylamine clusters, *The Journal*  
950 *of Chemical Physics* 2013 139:8, 2013.

951 Ortega, I. K., Kupiainen, O., Kurtén, T., Olenius, T., Wilkman, O., McGrath, M. J., Loukonen, V.,  
952 and Vehkamäki, H., From quantum chemical formation free energies to evaporation rates,  
953 *Atmos. Chem. Phys.*, 12, 225-235, 2012.

954 Payzant, J.D.; Cunningham, A.J.; Kebarle, P., Gas - Phase Solvation of Ammonium Ion by NH<sub>3</sub>  
955 and H<sub>2</sub>O and Stabilities of Mixed Clusters NH<sub>4</sub><sup>+</sup>(NH<sub>3</sub>)<sub>n</sub>(H<sub>2</sub>O)<sub>w</sub>, *Can. J. Chem.*, 51, 19, 3242,  
956 1973.

957 Peng, X.Q., Liu, Y.R., Huang, T., Jiang, S. and Huang, W., Interaction of gas phase oxalic acid  
958 with ammonia and its atmospheric implications, *Physical Chemistry Chemical Physics*, 17(14),  
959 9552-9563, 2015.

960 Raes, F., A. Janssens, and R. V. Dingenen, The role of ion-induced aerosol formation in the lower  
961 atmosphere, *J. Aerosol Sci.*, 17, 466–470, 1986.

962 Schnitzhofer, R., et al., Characterisation of organic contaminants in the CLOUD chamber at  
963 CERN, *Atmos. Meas. Tech.*, 7, 2159–2168, doi:10.5194/amt-7-2159-2014, 2014.

964 Schobesberger, S., et al., On the composition of ammonia–sulfuric-acid ion clusters during aerosol  
965 particle formation, *Atmos. Chem. Phys.*, 15, 55-78, <https://doi.org/10.5194/acp-15-55-2015>,  
966 2015.

967 Sipilä, M., Berndt, T., Petäjä, T., Brus, D., Vanhanen, J., Stratmann, F., Patokoski, J.,  
968 Mauldin, R. L., Hyvärinen, A. P., Lihavainen, H., and Kulmala, M.: The Role of  
969 Sulfuric Acid in Atmospheric Nucleation, *Science*, 327, 1243,  
970 <https://doi.org/10.1126/science.1180315>, 2010.

971 Sorokin, A., Arnold, F. and Wiedner, D., Formation and growth of sulfuric acid–water cluster ions:  
972 Experiments, modelling, and implications for ion-induced aerosol formation, *Atmospheric*  
973 *Environment*, 40, 2030-2045, 2006.

974 Temelso, B., Morrell, T.E., Shields, R.M., Allodi, M.A., Wood, E.K., Kirschner, K.N.,  
975 Castonguay, T.C., Archer, K.A. and Shields, G.C., Quantum mechanical study of sulfuric acid  
976 hydration: Atmospheric implications. *The Journal of Physical Chemistry A*, 116(9), 2209-2224,  
977 2012a.

978 Temelso, B., Phan, T.N. and Shields, G.C., Computational study of the hydration of sulfuric acid  
979 dimers: Implications for acid dissociation and aerosol formation, *Journal of Physical Chemistry*  
980 *A*, 116(39), pp.9745-9758, 2012b.

981 Thomson, J. J., *Applications of Dynamics to Physics and Chemistry*, 1st ed., Cambridge University  
982 Press, London, 1888.

983 Torpo, L., Kurtén, T., Vehkamäki, H., Laasonen, K., Sundberg, M.R. and Kulmala, M.,  
984 Significance of ammonia in growth of atmospheric nanoclusters. *The Journal of Physical*  
985 *Chemistry A*, 111(42), pp.10671-10674, 2007.

986 Vehkamäki H., Kulmala, M., Napari, I., Lehtinen, K. E. J., Timmreck, C., Noppel, M., and  
 987 Laaksonen, A., An improved parameterization for sulfuric acid–water nucleation rates for  
 988 tropospheric and stratospheric conditions, *J. Geophys. Res.*, 107 (D22), 4622,  
 989 doi:10.1029/2002JD002184, 2002.

990 Warner, J. X., Wei, Z., Strow, L. L., Dickerson, R. R., & Nowak, J. B.. The global tropospheric  
 991 ammonia distribution as seen in the 13-year AIRS measurement record. *Atmospheric Chemistry  
 992 and Physics*, 16(8), 5467-5479. <https://doi.org/10.5194/acp-16-5467-2016>, 2016.

993 Wilhelm, S., Eichkorn, S., Wiedner, D., Pirjola, L. and Arnold, F.: Ion-induced aerosol formation:  
 994 new insights from laboratory measurements of mixed cluster ions,  $\text{HSO}_4^-(\text{H}_2\text{SO}_4)_a(\text{H}_2\text{O})_w$  and  
 995  $\text{H}^+(\text{H}_2\text{SO}_4)_a(\text{H}_2\text{O})_w$ , *Atmos. Environ.*, 38, 1735-1744, 2004.

996 Włodek, S., Z. Łuczyński, H. Wincel, Stabilities of gas-phase  $\text{NO}_3^- (\text{HNO}_3)_n$ ,  $n \leq 6$ , clusters, In  
 997 *International Journal of Mass Spectrometry and Ion Physics*, 35, 1–2, 1980, 39-46, 1980.

998 Xu, W. and Zhang, R., A theoretical study of hydrated molecular clusters of amines and  
 999 dicarboxylic acids, *Journal of chemical physics*, 139(6), p.064312, 2013.

1000 Xu, W. and Zhang, R., Theoretical investigation of interaction of dicarboxylic acids with common  
 1001 aerosol nucleation precursors, *Journal of Physical Chemistry A*, 116(18), 4539-4550, 2012.

1002 Yu, F., and Turco, R. P., The role of ions in the formation and evolution of particles in aircraft  
 1003 plumes, *Geophys. Res. Lett.*, 24, 1927-1930, 1997.

1004 Yu, F., and Turco, R. P., Ultrafine aerosol formation via ion-mediated nucleation, *Geophys. Res.  
 1005 Lett.*, 27, 883-886, 2000.

1006 Yu, F., and R. P. Turco: From molecular clusters to nanoparticles: The role of ambient ionization  
 1007 in tropospheric aerosol formation, *J. Geophys. Res.*, 106, 4797-4814, 2001.

1008 Yu, F. and Turco, R. P., The size-dependent charge fraction of sub-3-nm particles as a key  
 1009 diagnostic of competitive nucleation mechanisms under atmospheric conditions, *Atmos. Chem.  
 1010 Phys.*, 11, 9451–9463, doi:10.5194/acp-11-9451-2011, 2011.

1011 Yu, F., Modified Kelvin-Thomson equation considering ion-dipole interaction: Comparison with  
 1012 observed ion-clustering enthalpies and entropies, *J. Chem. Phys.*, 122, 084503, 2005.

1013 Yu, F., Effect of ammonia on new particle formation: A kinetic  $\text{H}_2\text{SO}_4\text{-H}_2\text{O-NH}_3$  nucleation model  
 1014 constrained by laboratory measurements, *J. Geophys. Res.*, 111, D01204,  
 1015 doi:10.1029/2005JD005968, 2006a.

1016 Yu, F., From molecular clusters to nanoparticles: Second-generation ion-mediated nucleation  
 1017 model, *Atmos. Chem. Phys.*, 6, 5193-5211, 2006b.

1018 Yu, F., Improved quasi-unary nucleation model for binary  $\text{H}_2\text{SO}_4\text{-H}_2\text{O}$  homogeneous nucleation,  
 1019 *J. Chem. Phys.*, 127, 054301, 2007.

1020 Zhang, R, Khalizov, AF, Wang, L, Hu,M, Wen,X., Nucleation and growth of nanoparticles in the  
1021 atmosphere, Chem. Rev. 112: 1957-2011, DOI: 10.1021/cr2001756, 2012.

1022 Zhang, R., Wang, L., Khalizov, A.F., Zhao, J., Zheng, J., McGraw, R.L. and Molina, L.T.,  
1023 Formation of nanoparticles of blue haze enhanced by anthropogenic pollution, Proceedings of  
1024 the National Academy of Sciences, 106(42), 17650-17654, 2009.

1025 Zhang, Y., P. H. McMurry, F. Yu, and M. Z. Jacobson, A Comparative Study of Homogeneous  
1026 Nucleation Parameterizations, Part I. Examination and Evaluation of the Formulations, J.  
1027 Geophys. Res., 115, D20212, doi:10.1029/2010JD014150, 2010.

1028 Zhu, Y.P., Liu, Y.R., Huang, T., Jiang, S., Xu, K.M., Wen, H., Zhang, W.J. and Huang, W.,  
1029 Theoretical study of the hydration of atmospheric nucleation precursors with acetic acid, Journal  
1030 of Physical Chemistry A, 118(36), 7959-7974, 2014.

1031 Zollner, J. H., W. A. Glasoe, B. Panta, K. K. Carlson, P. H. McMurry, and D. R. Hanson, Sulfuric  
1032 acid nucleation: Power dependencies, variation with relative humidity, and effect of bases,  
1033 Atmos. Chem. Phys., 12(10), 4399–4411, doi:10.5194/acp-12-4399-2012, 2012.

1034

1035 **Table A1.** Number of isomers successfully converged at 6-311 level for selected clusters, along  
 1036 with the enthalpy, entropy, and Gibbs free energy of the most stable isomers.  
 1037

Cluster Formula	6-311++ conv.	Enthalpy (Hartree)	Entropy (cal/K·mol)	Gibbs free energy (Hartree)
S <sub>4</sub>	56	-2801.256008	179.461	-2801.341276
S <sub>4</sub> A <sub>1</sub>	169	-2857.820795	187.395	-2857.909833
S <sub>4</sub> A <sub>2</sub>	84	-2914.388489	193.997	-2914.480663
S <sub>4</sub> A <sub>3</sub>	68	-2970.94645	209.77	-2971.046119
S <sub>4</sub> A <sub>4</sub>	38	-3027.500303	225.959	-3027.607663
S <sub>4</sub> A <sub>5</sub>	34	-3084.050337	237.758	-3084.163303
S <sup>-</sup> S <sub>3</sub>	97	-2800.835072	168.993	-2800.915366
S <sup>-</sup> S <sub>3</sub> A <sub>1</sub>	122	-2857.389946	184.899	-2857.477797
S <sup>-</sup> S <sub>3</sub> A <sub>2</sub>	21	-2913.941409	192.489	-2914.032867
S <sup>-</sup> S <sub>3</sub> A <sub>3</sub>	13	-2970.490814	195.627	-2970.583762
S <sup>-</sup> S <sub>4</sub>	138	-3501.162655	200.525	-3501.257931
S <sup>-</sup> S <sub>4</sub> A <sub>1</sub>	71	-3557.727072	208.015	-3557.825907
S <sup>-</sup> S <sub>4</sub> A <sub>2</sub>	22	-3614.287482	213.397	-3614.388874
S <sup>-</sup> S <sub>4</sub> A <sub>3</sub>	23	-3670.836831	226.504	-3670.94445
S <sup>-</sup> S <sub>4</sub> A <sub>4</sub>	18	-3727.385956	237.152	-3727.498634
H <sup>+</sup> A <sub>2</sub>	16	-113.413269	68.478	-113.445805
H <sup>+</sup> A <sub>2</sub> W <sub>1</sub>	42	-189.845603	94.248	-189.890384
H <sup>+</sup> A <sub>2</sub> W <sub>2</sub>	56	-266.276653	113.49	-266.330576
H <sup>+</sup> A <sub>2</sub> W <sub>3</sub>	63	-342.706301	132.722	-342.769362
H <sup>+</sup> A <sub>2</sub> W <sub>4</sub>	114	-419.133157	160.449	-419.209391
H <sup>+</sup> A <sub>2</sub> W <sub>5</sub>	116	-495.567408	161.447	-495.644117
H <sup>+</sup> A <sub>2</sub> W <sub>6</sub>	70	-571.994961	175.085	-572.078149
H <sup>+</sup> A <sub>2</sub> W <sub>0</sub> S <sub>1</sub>	40	-813.745253	107.764	-813.796455
H <sup>+</sup> A <sub>2</sub> W <sub>1</sub> S <sub>1</sub>	173	-890.181285	121.33	-890.238933
H <sup>+</sup> A <sub>2</sub> W <sub>2</sub> S <sub>1</sub>	103	-966.618165	130.584	-966.680209
H <sup>+</sup> A <sub>2</sub> W <sub>3</sub> S <sub>1</sub>	169	-1043.047622	154.145	-1043.120861
H <sup>+</sup> A <sub>2</sub> W <sub>4</sub> S <sub>1</sub>	188	-1119.476882	177.051	-1119.561004
H <sup>+</sup> A <sub>2</sub> W <sub>5</sub> S <sub>1</sub>	178	-1195.90253	200.029	-1195.99757
H <sup>+</sup> A <sub>2</sub> W <sub>6</sub> S <sub>1</sub>	85	-1272.330781	215.117	-1272.43299

1038

1039 **Table A2.** QC-based stepwise Gibbs free energy change (in kcal/mol) for the addition of one  
 1040 water ( $\Delta G_{+W}^{\circ}$ ), ammonia ( $\Delta G_{+A}^{\circ}$ ), or sulfuric acid ( $\Delta G_{+S}^{\circ}$ ) molecule to form the given positively  
 1041 charged clusters under standard conditions, and the corresponding experimental data or semi-  
 1042 experimental estimates.  
 1043

	$\Delta G_{+W}^{\circ}$		$\Delta G_{+A}^{\circ}$		$\Delta G_{+S}^{\circ}$	
	QC	experimental	QC	experimental	QC	experimental
$H^+W_1S_1$					-28.59	-24.65 <sup>f</sup>
$H^+W_2S_1$	-15.66				-15.33	-13.76 <sup>f</sup>
$H^+W_3S_1$	-9.40				-10.12	-11.93 <sup>f</sup>
$H^+W_4S_1$	-7.83				-9.18	-9.71 <sup>f</sup>
$H^+W_5S_1$	-6.77	-5.79 <sup>a</sup>			-9.52	-9.82 <sup>f</sup>
$H^+W_6S_1$	-5.32	-4.24 <sup>a</sup>			-9.70	-9.94 <sup>f</sup>
$H^+W_7S_1$	-3.18	-3.28 <sup>a</sup>			-9.64	-9.96 <sup>f</sup>
$H^+W_8S_1$	-2.80	-2.67 <sup>a</sup>			-9.84	-10.10 <sup>f</sup>
$H^+W_9S_1$	-2.30	-2.12 <sup>a</sup>			-10.24	-10.86 <sup>f</sup>
$H^+A_1W_1$	-13.47	-13.01 <sup>b</sup> , -11.43 <sup>c</sup>	-52.08			
$H^+A_1W_2$	-9.85	-7.14 <sup>b</sup> , -8.17 <sup>c</sup>	-33.02			
$H^+A_1W_3$	-6.60	-5.92 <sup>b</sup> , -5.88 <sup>c</sup>	-25.01			
$H^+A_1W_4$	-3.50	-3.94 <sup>b</sup> , -4.06 <sup>c</sup>	-19.73			
$H^+A_1W_5$	-2.50	-2.55 <sup>b</sup> , -3.02 <sup>c</sup>	-15.80			
$H^+A_1W_6$	-2.26	-2.54 <sup>b</sup>	-12.93			
$H^+A_1W_7$	-1.15	-1.84 <sup>b</sup>	-10.84			
$H^+A_1W_8$	-1.02		-9.26			
$H^+A_1W_9$	0.25		-8.32			
$H^+A_2$			-22.97	-18.25 <sup>c</sup>		
$H^+A_2W_1$	-7.04	-6.85 <sup>c</sup>	-16.53	-11.54 <sup>c</sup> , -12.75 <sup>d</sup>		
$H^+A_2W_2$	-4.29	-5.25 <sup>c</sup>	-10.97	-9.13 <sup>c</sup> , -9.50 <sup>d</sup>		
$H^+A_2W_3$	-3.41	-3.70 <sup>c</sup>	-7.78	-6.83 <sup>c</sup> , -7.02 <sup>d</sup>		
$H^+A_2W_4$	-3.08		-7.36			
$H^+A_2W_5$	-1.97		-6.82			
$H^+A_2W_6$	-0.42		-4.99			
$H^+A_1W_1S_1$	-8.99		-33.14		-9.65	-8.3 <sup>d</sup>
$H^+A_1W_2S_1$	-8.11		-25.59		-7.90	-7.1 <sup>d</sup>
$H^+A_1W_3S_1$	-6.09		-22.28		-7.40	-6.7 <sup>d</sup>
$H^+A_1W_4S_1$	-4.25		-18.71		-8.15	-6.9 <sup>d</sup>
$H^+A_1W_5S_1$	-1.92		-13.85		-7.56	-7.5 <sup>d</sup>
$H^+A_1W_6S_1$	-2.04		-10.57		-7.34	-8.0 <sup>d</sup>
$H^+A_2W_0S_1$			-22.09	-22.14 <sup>e</sup>	-13.35	-16.8 <sup>d</sup>

H <sup>+</sup> A <sub>2</sub> W <sub>1</sub> S <sub>1</sub>	-5.72	-18.92	-12.03	-15.8 <sup>d</sup>
H <sup>+</sup> A <sub>2</sub> W <sub>2</sub> S <sub>1</sub>	-4.97	-15.78	-12.71	-15.9 <sup>d</sup>
H <sup>+</sup> A <sub>2</sub> W <sub>3</sub> S <sub>1</sub>	-4.58	-14.27	-13.89	-16.3 <sup>d</sup>
H <sup>+</sup> A <sub>2</sub> W <sub>4</sub> S <sub>1</sub>	-4.26	-14.27	-15.06	-17.3 <sup>d</sup>
H <sup>+</sup> A <sub>2</sub> W <sub>5</sub> S <sub>1</sub>	-2.01	-14.37	-15.11	-18.8 <sup>d</sup>
H <sup>+</sup> A <sub>2</sub> W <sub>6</sub> S <sub>1</sub>	-1.29	-13.63	-15.98	-19.9 <sup>d</sup>

---

1044 <sup>a</sup> Froyd and Lovejoy, 2003; <sup>b</sup> Meot-Ner (Mautner) et al., 1984; <sup>c</sup> Payzant et al., 1973; <sup>d</sup> Froyd, 2002; <sup>e</sup>

1045 Froyd and Lovejoy, 2012. <sup>f</sup> The  $\Delta G_{+S}^{\circ}$  values given here were calculated based on experimental  $\Delta G_{+S}^{\circ}$

1046 values at T=270 K from Froyd and Lovejoy (2003) and  $\Delta S$  values from quantum calculation.

1047



1048 **Table A3.** Same as Table A2 except for neutral clusters.

1049

	$\Delta G_{+W}^{\circ}$		$\Delta G_{+A}^{\circ}$		$\Delta G_{+S}^{\circ}$	
	QC	experimental	QC	experimental	QC	experimental
S <sub>1</sub> A <sub>1</sub>			-7.77 <sup>a</sup> (-7.29 <sup>b</sup> , -7.61 <sup>c</sup> , -6.60 <sup>d</sup> )	-8.2 <sup>e</sup>	-7.77 <sup>a</sup> (-7.29 <sup>b</sup> , -7.61 <sup>c</sup> , -6.60 <sup>d</sup> )	-8.2 <sup>e</sup>
S <sub>1</sub> A <sub>1</sub> W <sub>1</sub>	-1.39 <sup>a</sup>		-6.88 <sup>a</sup>			
S <sub>1</sub> A <sub>1</sub> W <sub>2</sub>	-2.30 <sup>a</sup>		-6.18 <sup>a</sup>			
S <sub>1</sub> A <sub>1</sub> W <sub>3</sub>	-1.52 <sup>a</sup>		-5.81 <sup>a</sup>			
S <sub>1</sub> A <sub>2</sub>			-4.75			
S <sub>1</sub> A <sub>2</sub> W <sub>1</sub>	-0.78		-4.15			
S <sub>2</sub> A <sub>1</sub>			-13.84 <sup>a</sup>		-11.65 <sup>a</sup>	
S <sub>2</sub> A <sub>1</sub> W <sub>1</sub>	-2.31 <sup>a</sup>		-12.77		-12.59 <sup>a</sup>	
S <sub>2</sub> A <sub>1</sub> W <sub>2</sub>	-1.21 <sup>a</sup>		-11.00		-11.52 <sup>a</sup>	
S <sub>2</sub> A <sub>1</sub> W <sub>3</sub>	-2.04 <sup>a</sup>		-9.69		-12.04 <sup>a</sup>	
S <sub>2</sub> A <sub>2</sub>			-8.75		-15.65	
S <sub>2</sub> A <sub>2</sub> W <sub>1</sub>	-1.96		-8.37		-16.83	
S <sub>2</sub> A <sub>2</sub> W <sub>2</sub>	-1.19		-8.35		-15.49	
S <sub>2</sub> A <sub>2</sub> W <sub>3</sub>	0.60		-5.71		-14.42	
S <sub>2</sub> A <sub>3</sub>			-4.19			
S <sub>3</sub> A <sub>1</sub>			-16.14		-7.08	
S <sub>3</sub> A <sub>2</sub>			-13.84		-12.17	
S <sub>3</sub> A <sub>3</sub>			-8.93		-16.92	
S <sub>3</sub> A <sub>4</sub>			-7.42			
S <sub>4</sub> A <sub>1</sub>			-15.74		-4.16	
S <sub>4</sub> A <sub>2</sub>			-17.16		-7.48	
S <sub>4</sub> A <sub>3</sub>			-13.79		-12.34	
S <sub>4</sub> A <sub>4</sub>			-11.34		-16.26	
S <sub>4</sub> A <sub>5</sub>			-7.63			

1050 <sup>a</sup> Nadykto and Yu, 2007; <sup>b</sup> Torpo et al., 2007; <sup>c</sup> Ortega et al., 2012; <sup>d</sup> Chon et al., 2007; <sup>e</sup> Kurten et al.,  
 1051 2015.

1052

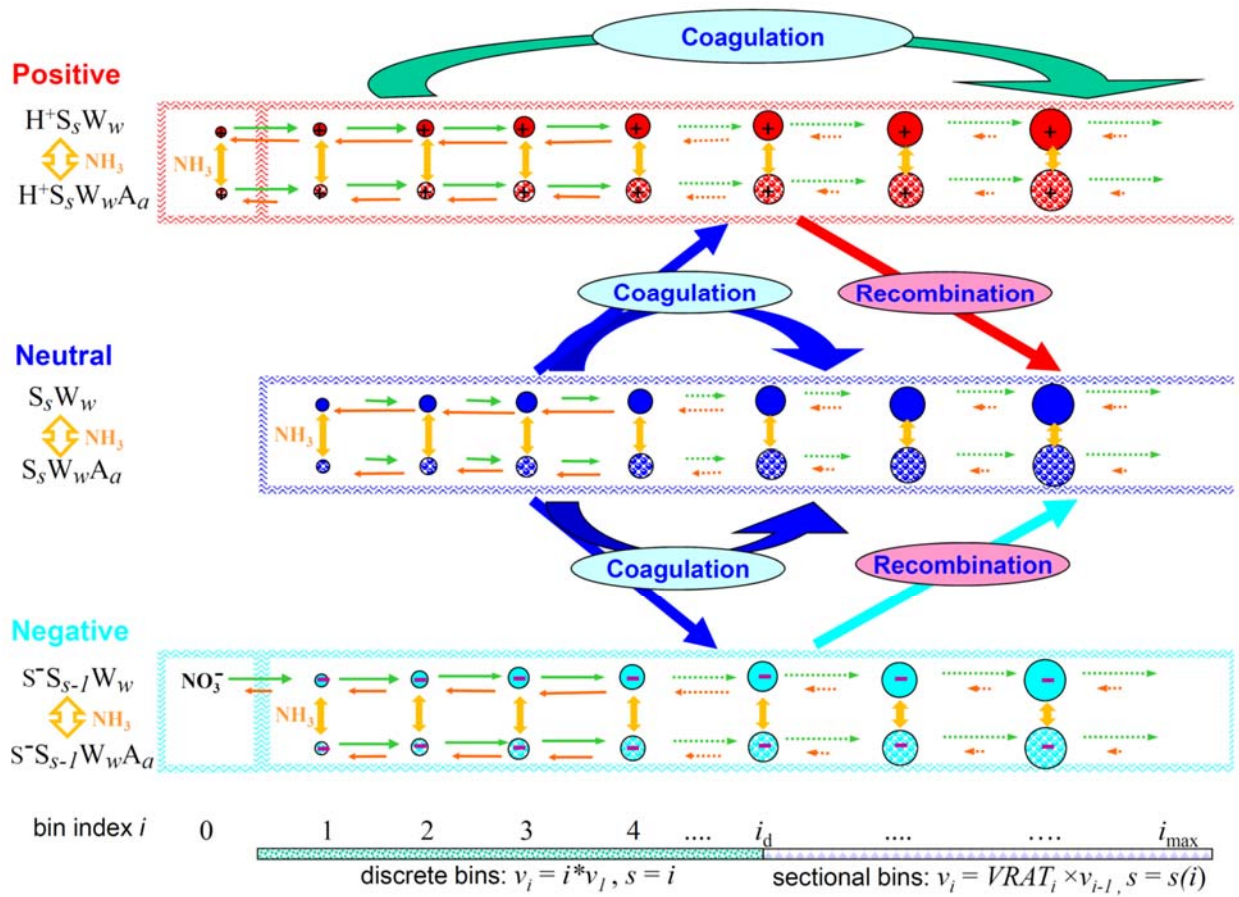
1053 **Table A4.** Same as Table A2 except for negatively charged clusters.

1054

	$\Delta G_{+W}^{\circ}$		$\Delta G_{+\Delta}^{\circ}$		$\Delta G_{+S}^{\circ}$	
	QC	experimental	QC	experimental	QC	experimental
S <sup>-</sup> A <sub>1</sub>			2.81			
S <sup>-</sup> S <sub>1</sub> W <sub>0</sub>					-32.74	-29.10 <sup>a</sup>
S <sup>-</sup> S <sub>1</sub> W <sub>1</sub>	-0.61				-28.12	
S <sup>-</sup> S <sub>1</sub> W <sub>2</sub>	-1.06				-25.36	
S <sup>-</sup> S <sub>1</sub> A <sub>1</sub>			0.08		-35.47	
S <sup>-</sup> S <sub>2</sub> W <sub>0</sub>					-15.06	-17.14 <sup>a</sup>
S <sup>-</sup> S <sub>2</sub> W <sub>1</sub>	-1.83				-16.28	
S <sup>-</sup> S <sub>2</sub> A <sub>1</sub>			-4.85		-19.99	
S <sup>-</sup> S <sub>3</sub> W <sub>0</sub>					-10.58	-13.28 <sup>a</sup>
S <sup>-</sup> S <sub>3</sub> W <sub>1</sub>	-2.92	-2.73 <sup>a</sup>			-11.67	-14.29 <sup>a</sup>
S <sup>-</sup> S <sub>3</sub> W <sub>2</sub>	-2.03	-1.53 <sup>a</sup>			-11.12	-13.80 <sup>a</sup>
S <sup>-</sup> S <sub>3</sub> W <sub>3</sub>	-2.01	-1.93 <sup>a</sup>			-11.52	-14.72 <sup>a</sup>
S <sup>-</sup> S <sub>3</sub> W <sub>4</sub>	-1.73					
S <sup>-</sup> S <sub>3</sub> A <sub>1</sub> W <sub>0</sub>			-11.89		-17.62	
S <sup>-</sup> S <sub>3</sub> A <sub>1</sub> W <sub>1</sub>	0.52		-8.45		-14.90	
S <sup>-</sup> S <sub>3</sub> A <sub>1</sub> W <sub>2</sub>	0.39		-6.03		-13.06	
S <sup>-</sup> S <sub>3</sub> A <sub>2</sub>			-7.27		-18.36	
S <sup>-</sup> S <sub>3</sub> A <sub>3</sub>			-4.66			
S <sup>-</sup> S <sub>4</sub> W <sub>0</sub>					-8.28	-10.96 <sup>a</sup>
S <sup>-</sup> S <sub>4</sub> W <sub>1</sub>	-3.50	-2.61 <sup>a</sup>			-8.86	-10.71 <sup>a</sup>
S <sup>-</sup> S <sub>4</sub> W <sub>2</sub>	-3.17	-2.79 <sup>a</sup>			-9.99	-12.10 <sup>a</sup>
S <sup>-</sup> S <sub>4</sub> W <sub>3</sub>	-2.65	-2.41 <sup>a</sup>			-10.64	-12.48 <sup>a</sup>
S <sup>-</sup> S <sub>4</sub> W <sub>4</sub>	-2.25	-2.14 <sup>a</sup>			-11.16	-12.77 <sup>a</sup>
S <sup>-</sup> S <sub>4</sub> A <sub>1</sub> W <sub>0</sub>			-15.37		-11.76	
S <sup>-</sup> S <sub>4</sub> A <sub>1</sub> W <sub>1</sub>	-2.21		-14.09		-14.49	
S <sup>-</sup> S <sub>4</sub> A <sub>1</sub> W <sub>2</sub>	-0.74		-11.66		-15.62	
S <sup>-</sup> S <sub>4</sub> A <sub>2</sub>			-12.23		-16.71	
S <sup>-</sup> S <sub>4</sub> A <sub>3</sub>			-7.59		-19.65	
S <sup>-</sup> S <sub>4</sub> A <sub>4</sub>			-6.72			

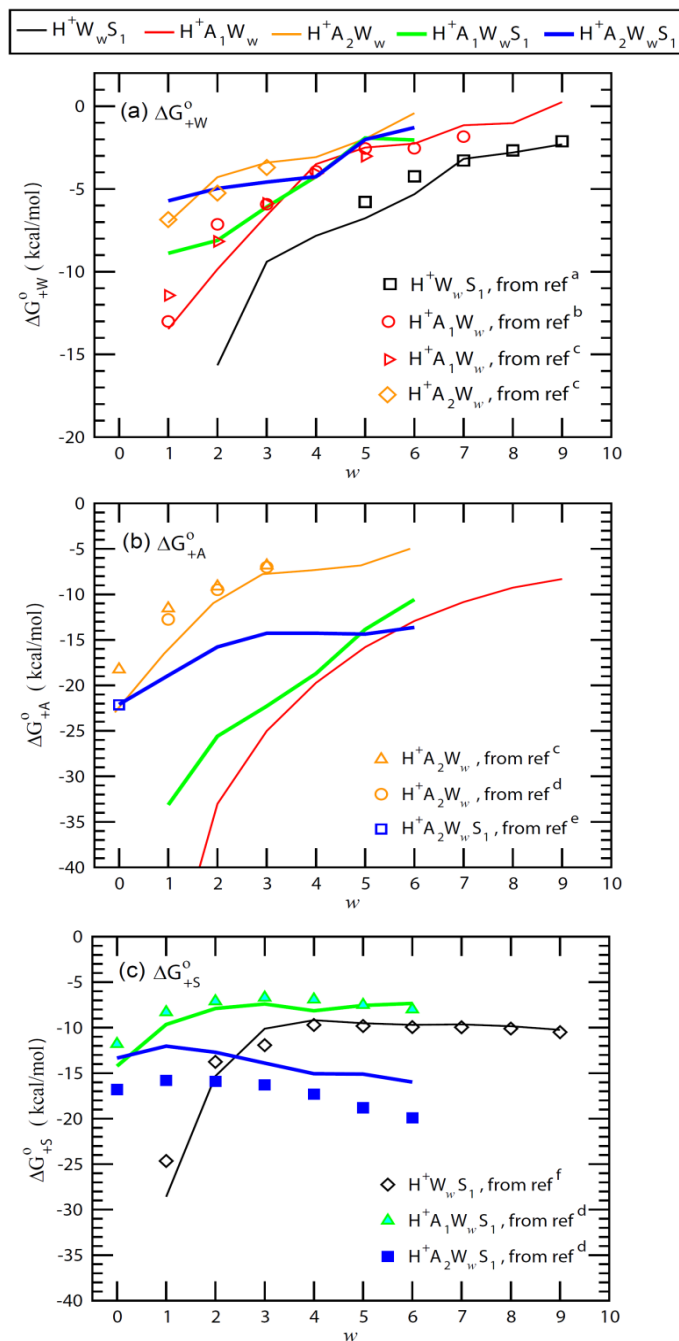
1055 <sup>a</sup> Froyd and Lovejoy, 2003.

1056

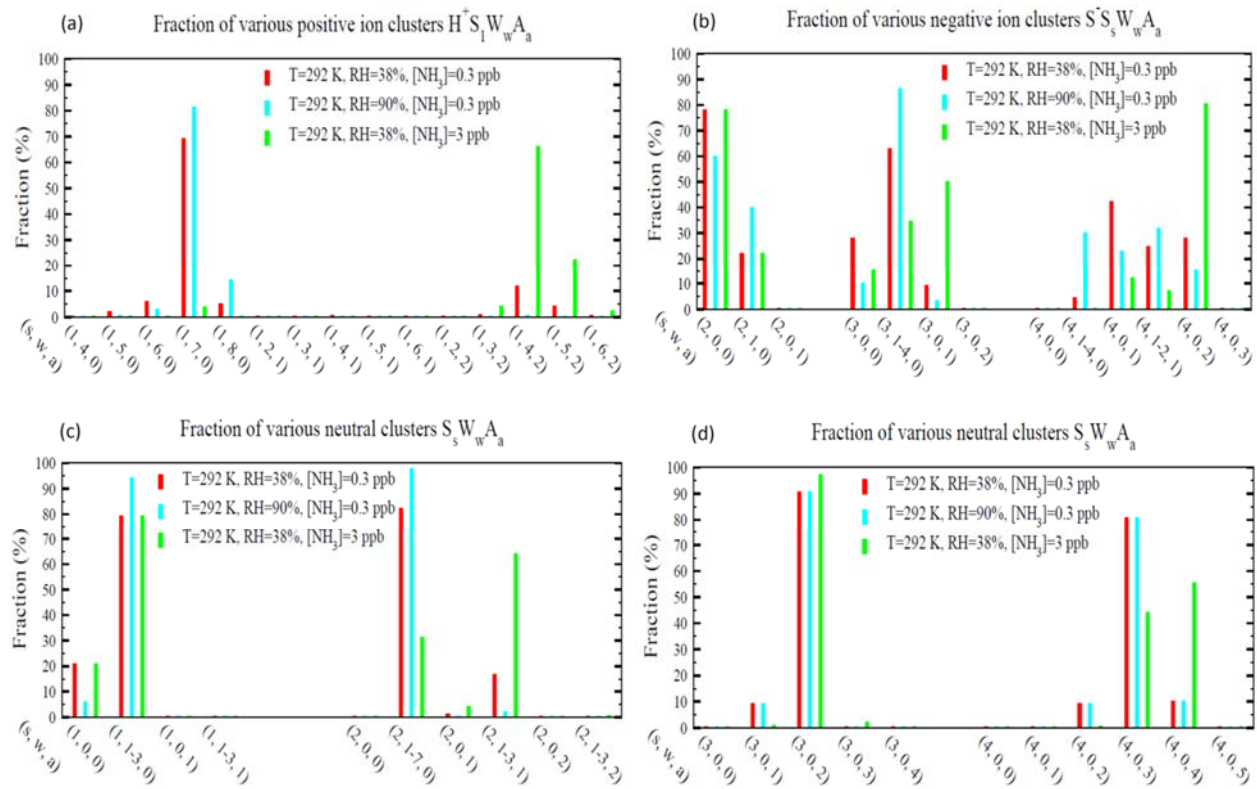


1057  
1058

1059 **Figure 1.** Schematic illustration of kinetic processes controlling the evolution of positively  
 1060 charged ( $H^+S_sW_wA_a$ ), neutral ( $S_sW_wA_a$ ), and negatively charged ( $S^-S_{s-1}W_wA_a$ )  
 1061 clusters/droplets that are explicitly simulated in the ternary ion-mediated nucleation (TIMN)  
 1062 model. Here S, W, and A represent sulfuric acid ( $H_2SO_4$ ), water ( $H_2O$ ), and ammonia ( $NH_3$ )  
 1063 respectively, while  $s$ ,  $w$ , and  $a$  refer to the number of S, W, and A molecules in the clusters/droplets,  
 1064 respectively. The TIMN model has been extended from an earlier version treating binary IMN  
 1065 (BIMN) by adding  $NH_3$  into the nucleation system and using a discrete-sectional bin structure to  
 1066 represent the sizes of clusters/particles starting from a single molecule up to background particles  
 1067 larger than a few micrometers.



1068  
 1069 **Figure 2.** Stepwise Gibbs free energy change under standard conditions for the addition of a water  
 1070 ( $\Delta G^\circ_{+W}$ ), ammonia ( $\Delta G^\circ_{+A}$ ), or sulfuric acid ( $\Delta G^\circ_{+S}$ ) molecule to form the given positively charged  
 1071 clusters as a function of the number of water molecules in the clusters ( $w$ ). Lines are QC-based  
 1072 values, and symbols are experimental results or semi-experimental estimates (see notes under  
 1073 Table A2 for the references).



1075

1076

1077

1078

1079

1080

1081

1082

1083

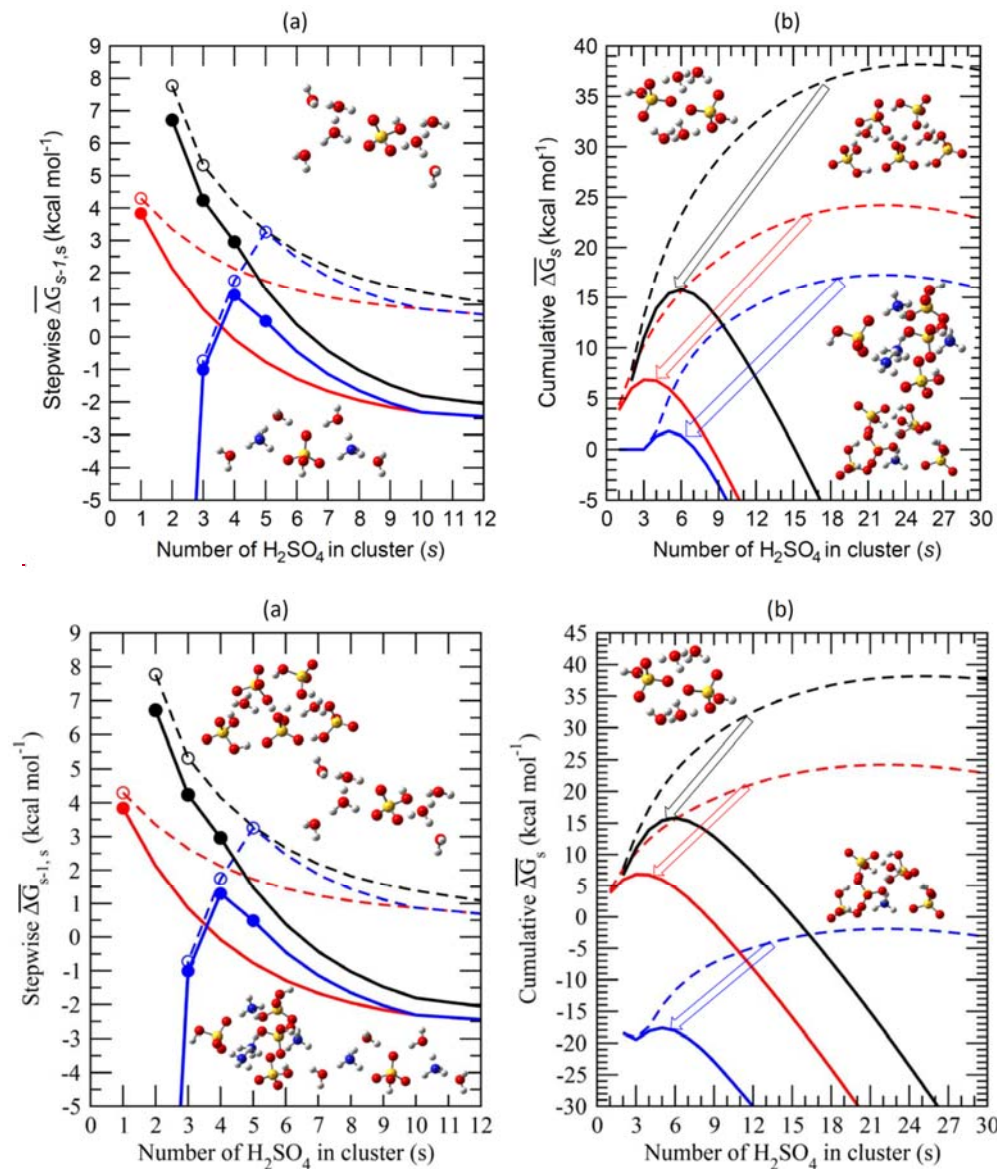
1084

**Figure 3.** Relative abundance (or molar fraction) of small clusters containing a given number of H<sub>2</sub>SO<sub>4</sub> molecules for positive, negative, and neutral cluster types at a temperature of 292 K and three different combinations of RHs (38% and 90%) and [NH<sub>3</sub>] (0.3 and 3 ppb). Some clusters with different numbers of water molecules were grouped together to make the plot more clear and neat. For the clusters shown in panel (d), there is no hydrate data and thus hydration for these clusters were not calculated.

1085

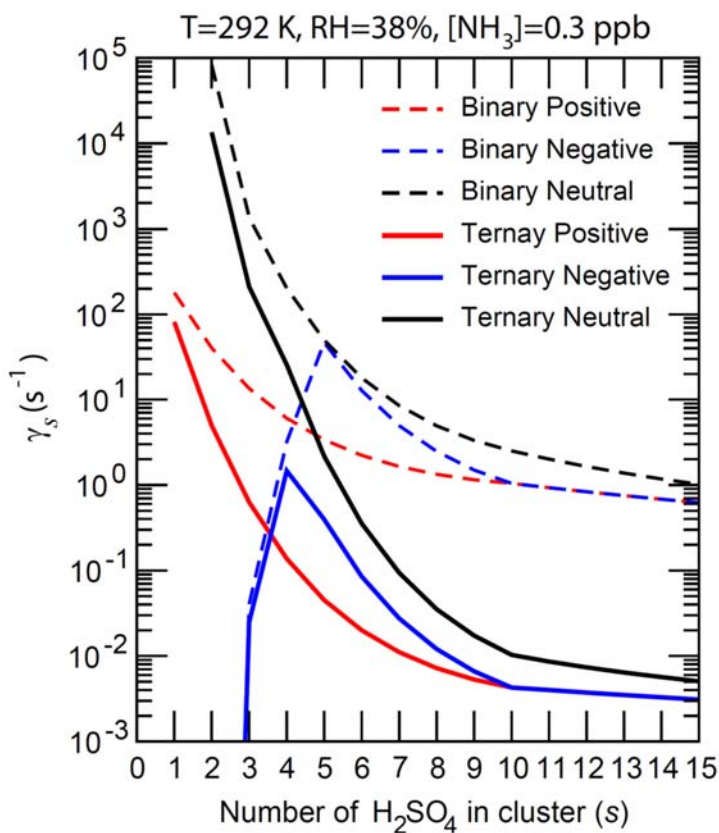
1086

1087



1088 **Figure 4.** (a) Average stepwise Gibbs free energy change for the addition of one H<sub>2</sub>SO<sub>4</sub> molecule  
 1089 to form a neutral (black), positively charged (red), or negatively charged (blue) binary H<sub>2</sub>SO<sub>4</sub>-H<sub>2</sub>O  
 1090 (dashed lines or empty circles) or ternary H<sub>2</sub>SO<sub>4</sub>-H<sub>2</sub>O-NH<sub>3</sub> (solid lines or filled circles) cluster  
 1091 containing *s* H<sub>2</sub>SO<sub>4</sub> molecules ( $\overline{\Delta G_{s-1,s}}$ ); (b) Same as (a) but for the cumulative (total) Gibbs free  
 1092 energy change in each case. Filled and empty circles in (a) refer to  $\overline{\Delta G_{s-1,s}}$  obtained using

1093 measurements and/or quantum-chemical calculations.  $\overline{\Delta G}_{s-1,s}$  for larger clusters with  $s \geq 10$ , which  
 1094 approach the properties of the equivalent bulk liquid (20), are calculated using the capillarity  
 1095 approximation. Interpolation is used to calculate  $\overline{\Delta G}_{s-1,s}$  for clusters up to  $s=10$  (Eq. 11).  
 1096 Calculations were carried out at  $T=292$  K,  $RH=38\%$ ,  $[H_2SO_4]=3 \times 10^8 \text{ cm}^{-3}$  and  $[NH_3]=0.3$  ppb.  
 1097 The inset diagrams represent equilibrium geometries for the most stable isomers of selected binary  
 1098 clusters (  $(H_3O^+)(H_2SO_4)(H_2O)_6$ ,  $(H_2SO_4)_2(H_2O)_4$ , and  $(HSO_4^-)(H_2SO_4)_4(H_2O)_2$  ), and ternary  
 1099 clusters (  $(NH_4^+)(H_2SO_4)(NH_3)(H_2O)_4$ ,  $(HSO_4^-)(H_2SO_4)_4(H_2O)(NH_3)$ ,  $(H_2SO_4)_4(NH_3)_4$  ).



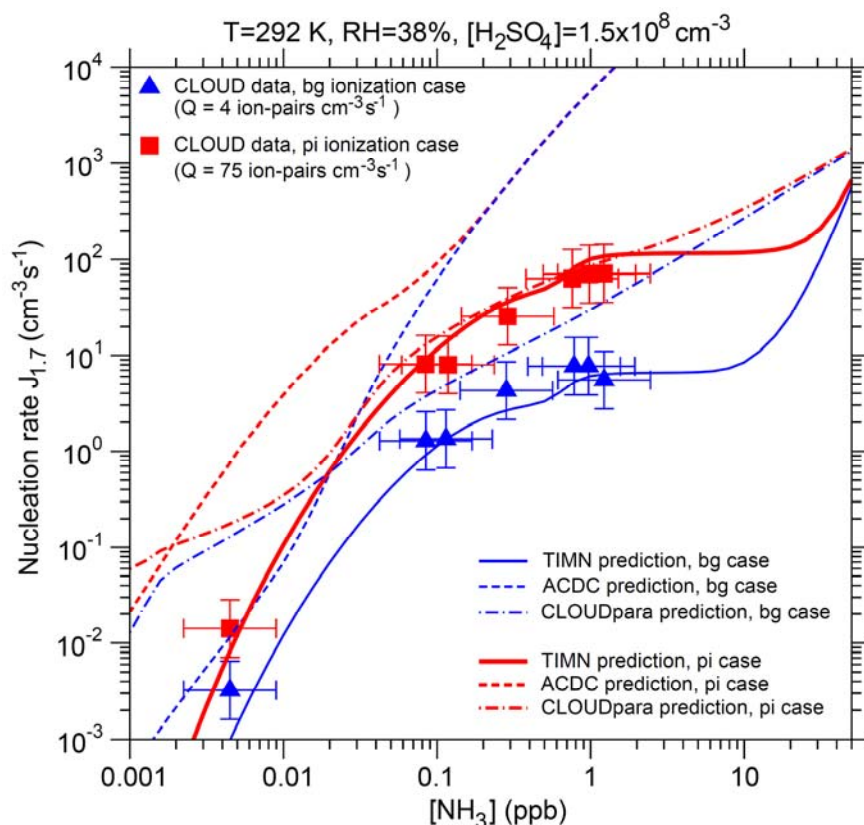
1100  
 1101 **Figure 5.** The number-concentration-weighted mean evaporation rates ( $\bar{\gamma}$ ) of  $H_2SO_4$  molecules  
 1102 from neutral clusters (black), positively charged clusters (red), and negatively charged clusters  
 1103 (blue) for binary ( $H_2SO_4$ - $H_2O$ , dashed lines) and ternary ( $H_2SO_4$ - $H_2O$ - $NH_3$ , solid lines) nucleating

1104 systems containing  $s$   $\text{H}_2\text{SO}_4$  molecules ( $\overline{\Delta G_{s-1,s}}$ ).  $T=292$  K,  $\text{RH}=38\%$ , and  $[\text{NH}_3] = 0.3$  ppb for  
 1105 the ternary system.

1106

1107

1108

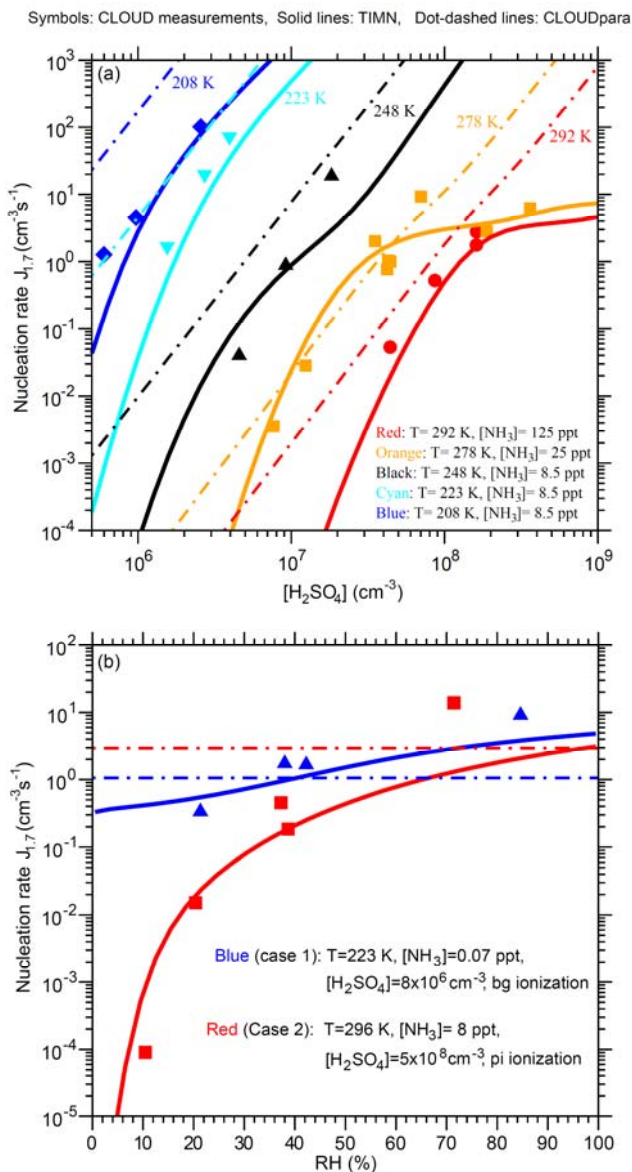


1109

1110 **Figure 6.** Effect of ammonia concentrations ( $[\text{NH}_3]$ ) on effective nucleation rates calculated at a  
 1111 cluster mobility diameter of 1.7 nm ( $J_{1.7}$ , lines) under the stated conditions with two ionization  
 1112 rates ( $Q$ ) – background ionization, bg (blue), and ionization enhanced by a pion beam, pi (red).  
 1113 Also shown are predictions from the TIMN model, the Atmospheric Cluster Dynamics Code  
 1114 (ACDC) with thermochemistry obtained using RI-CC2//B3LYP method (McGrath et al., 2012;  
 1115 Kurten et al., 2016), and an empirical parameterization of CLOUD measurements (CLOUDpara)  
 1116 (Dunne et al., 2016) are indicated by solid, dashed, and dot-dashed lines, respectively. The symbols  
 1117 refer to CLOUD experimental data (Kirkby et al., 2011; Dunne et al., 2016), with the uncertainties  
 1118 in measured  $[\text{NH}_3]$  and  $J_{1.7}$  shown by horizontal and vertical bars, respectively. To be comparable,

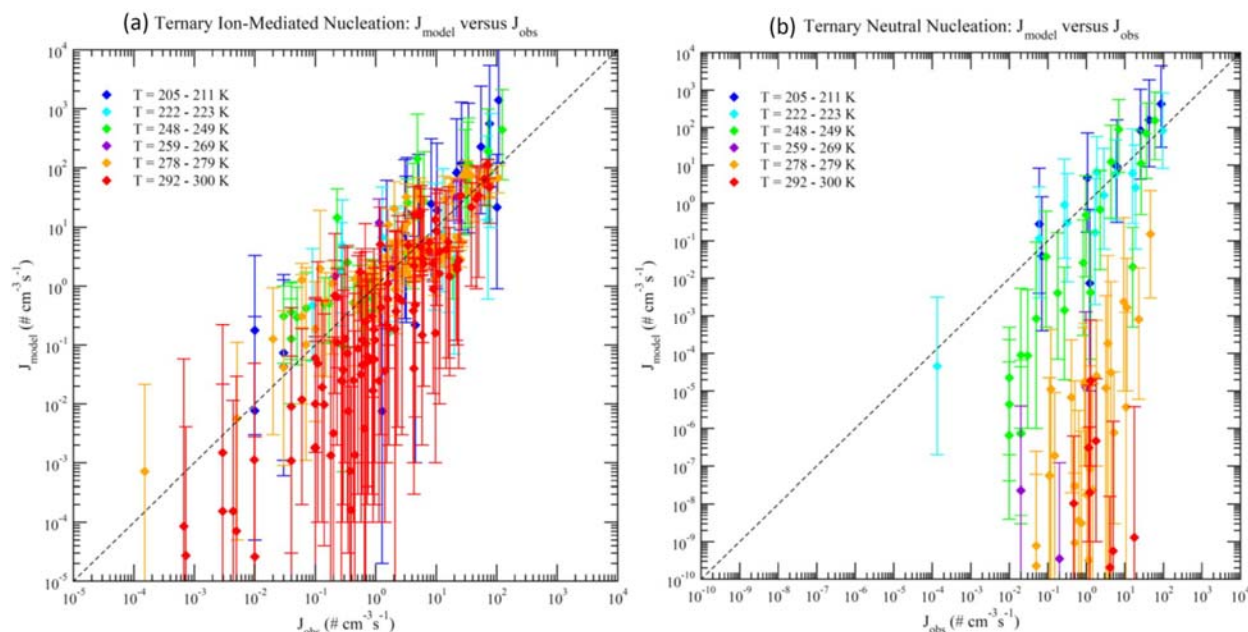


1119 the CLOUD data points given in Dunne et al. (2016) under the conditions of  $T=292$  K and  
 1120  $RH=38\%$  with  $[H_2SO_4]$  close to  $1.5 \times 10^8 \text{ cm}^{-3}$  have been interpolated to the same  $[H_2SO_4]$  value  
 1121 ( $=1.5 \times 10^8 \text{ cm}^{-3}$ ).



1122  
 1123 **Figure 7.** Comparison of TIMN simulations (solid lines), CLOUDpara predictions (Dunne et al.,  
 1124 2016) (dot-dashed lines) and CLOUD measurements (symbols, data from Dunne et al. (2016) of  
 1125 the dependences of nucleation rates on (a)  $[H_2SO_4]$  at five different temperatures ( $T=292$ , 278,  
 1126 248, 223, and 208 K) and (b) RH at two sets of conditions as specified.  $[NH_3]$  is in ppt (parts per  
 1127 trillion, by volume). Error bars for the uncertainties in measured  $[H_2SO_4]$  (-50%, +100%),  $[NH_3]$   
 1128 (-50%, +100%), and  $J_{1.7}$  (overall a factor of two) are not shown. To be comparable, the CLOUD  
 1129 data points given in Dunne et al. (2016) under the conditions ( $T$ , RH, ionization rate) with  $[NH_3]$

1130 or  $[\text{H}_2\text{SO}_4]$  close to the corresponding values specified in the figure legends have been interpolated  
 1131 to the same  $[\text{NH}_3]$  (Fig. 7a) or  $[\text{H}_2\text{SO}_4]$  (Fig. 7b) values.  
 1132  
 1133



1134  
 1135 **Figure 8.** Model predicted ( $J_{\text{model}}$ ) versus observed ( $J_{\text{obs}}$ ) nucleation rates under various conditions  
 1136 of all 377 data points of CLOUD measurements reported in Table S1 of Dunne et al. (2016), with  
 1137 (a) and without (b) the presence of ionization. The data points are grouped according to  
 1138 temperatures as specified in the legend. Vertical error bars show the range of  $J_{\text{model}}$  calculated at  
 1139 50% and 200% of measured  $[\text{H}_2\text{SO}_4]$ , corresponding to the uncertainties in measured  $[\text{H}_2\text{SO}_4]$  (-  
 1140 50%, +100%). Error bars associated with the uncertainties in measured  $[\text{NH}_3]$  (-50%, +100%), and  
 1141  $J_{\text{obs}}$  (overall a factor of two) are not shown.